SEDIMENTOLOGY the journal of the International Association of Sedimentologists

Sedimentology (2019) doi: 10.1111/sed.12571

Estuarine clay mineral distribution: Modern analogue for ancient sandstone reservoir quality prediction

JOSHUA GRIFFITHS*†, RICHARD H. WORDEN*, LUKE J. WOOLDRIDGE*‡, JAMES E. P. UTLEY*, ROBERT A. DULLER* and RHIANNON L. EDGE§
**Department of Earth, Ocean and Ecological Sciences, University of Liverpool, 4 Brownlow Street, Liverpool, L69 3GP, UK (E-mail: joshua.griffiths@BP.com)*
†BP Exploration, Chertsey Road, Sunbury-on-Thames, Middlesex, TW16 7LN, UK
‡BP Upstream Technology, Chertsey Road, Sunbury-on-Thames, Middlesex, TW16 7LN, UK
§Department of Health and Medicine, Lancaster University, Bailrigg, Lancaster, LA1 4YW, UK

Associate Editor – John Howell

ABSTRACT

The spatial distribution of clay minerals in sandstones, which may both enhance or degrade reservoir quality, is poorly understood. To address this, clay mineral distribution patterns and host-sediment properties (grain size, sorting, clay fraction abundance and bioturbation intensity) have, for the first time, been determined and mapped at an unprecedentedly high-resolution in a modern estuarine setting (Ravenglass Estuary, UK). Results show that the estuary sediment is dominated by illite with subordinate chlorite and kaolinite, although the rivers supply sediment with less illite and significantly more chlorite than found in the estuary. Fluvial-supplied sediment has been locally diluted by sediment derived from glaciogenic drift deposits on the margins of the estuary. Detailed clay mineral maps and statistical analyses reveal that the estuary has a heterogeneous distribution of illite, chlorite and kaolinite. Chlorite is relatively most abundant on the northern foreshore and backshore and is concentrated in coarse-grained inner estuary dunes and tidal bars. Illite is relatively most abundant (as well as being most crystalline and most Fe–Mg-rich) in fine-grained inner estuary and central basin mud and mixed flats. Kaolinite has the highest abundance in fluvial sediment and is relatively homogenous in tidally-influenced environments. Clay mineral distribution patterns in the Ravenglass Estuary have been strongly influenced by sediment supply (residence time) and subsequently modified by hydrodynamic processes. There is no relationship between macro-faunal bioturbation intensity and the abundance of chlorite, illite or kaolinite. Based on this modern-analogue study, outer estuarine sediments are likely to be heavily quartz cemented in deeply-buried (burial temperatures exceeding 80 to 100°C) sandstone reservoirs due to a paucity of clay grade material (<0·5%) to form complete grain coats. In contrast, chlorite-enriched tidal bars and dunes in the inner estuary, with their well-developed detrital clay coats, are likely to have quartz cement inhibiting authigenic clay coats in deeply-buried sandstones.

Keywords Clay mineral, estuary, modern, prediction, sandstone reservoir quality.

INTRODUCTION

Clay minerals may enhance or degrade sandstone reservoir quality, depending on type and abundance. For example, pore-filling illite significantly lowers permeability, whilst grain-coating chlorite may preserve porosity through the inhibition of pore-filling quartz cement (Ehrenberg, 1993; Ajdukiewicz & Larese, 2012; Stricker & Jones, 2016; Skarpeid *et al.*, 2017; Griffiths *et al.*, 2018a,b). Chlorite grain coats are found in sandstones deposited in a range of depositional environments but are especially common in marginal marine settings (Dowey *et al.*, 2012). Despite growing interest in the petroleum industry, there is no workflow to predict the spatial and stratigraphic distribution of clay minerals in the subsurface.

Volumes of sediment, modern or ancient (as sedimentary rock), are rarely homogeneous; instead they typically display significant heterogeneities in terms of total clay content, primary grain mineralogy, grain size and grain sorting, and varying degrees of bioturbation, soil development and infiltration. It can also be anticipated that the relative abundance of specific types of clay minerals are not homogeneously distributed throughout modern and ancient sand bodies. Note that this article carefully discriminates between the term 'clay mineral', referring to aluminium-rich sheet silicate minerals (phyllosilicates) and the term 'clay', referring to sediment particles that are smaller than 2 μm in size. With reference to modern marginal marine environments, while it is possible to start to predict the distribution of clay grade material (Dalrymple *et al.*, 1992; Dowey *et al.*, 2017; Wooldridge *et al.*, 2017a,b; Griffiths *et al.*, 2018b; Virolle *et al.*, 2018), it is not possible to identify areas of enrichment of one specific clay mineral (for example, chlorite) relative to other clay minerals. Fundamentally, there is a lack of knowledge and understanding on how specific clay minerals are distributed in most modern sedimentary environments and in ancient, deeply buried sandstone reservoirs.

Diagenetic clay coats in sandstones may originate from the thermally-driven recrystallization of low-temperature detrital clay coats, or through *in situ* growth from the authigenic alteration of precursor and early-diagenetic minerals, which interact with pore fluids during burial (Hillier, 1994; Aagaard *et al.*, 2000; Worden & Morad, 2003; Ajdukiewicz & Larese, 2012). As a result, to facilitate improved reservoir quality prediction, a new focus has arisen on the use of modern analogues to understand the origin, distribution and variable extent of detrital clay coats in clastic systems (Dowey *et al.*, 2017; Jones, 2017; Wooldridge *et al.*, 2017a,b; Griffiths *et al.*, 2018b; Virolle *et al.*, 2018). However, in addition to the extent and completeness (i.e. fraction of the sand grain-surface covered by clay minerals) of a clay coat, the mineralogy also exerts a strong control on the ability of clay coated sand grains to inhibit quartz cementation (Bloch *et al.*, 2002; Billault *et al.*, 2003; Lander *et al.*, 2008; Ajdukiewicz & Larese, 2012). Consequently, there is an additional need to map out clay mineral distribution patterns and understand the dominant controls on clay mineral distribution patterns at a scale relevant to oil and gas reservoirs. The primary objective of this study is to better understand the distribution of clay minerals in an estuary, which will enable the prediction of clay mineral type, abundance and distribution in ancient marginal-marine sandstones.

In order to implement modern analogue studies of clay mineral distribution patterns, to facilitate improved prediction of authigenic clay coat and clay mineral distribution patterns in petroleum reservoirs, typical burial diagenetic pathways need to first be considered. Even during the long timescale of burial diagenesis, the main components of clay minerals (for chlorite: Fe-oxides, Al-oxides and Si-oxides) have extremely low aqueous solubility and therefore clay mineral, and especially chlorite, diagenesis during burial can be assumed to be an isochemical process; i.e. closed-system diagenesis (Worden & Morad, 2003; Worden *et al.*, 2018). Chlorite, and possibly other clay mineral presence, is thus not the result of mass influx of materials into sandstones during diagenesis, rather it represents either primary chlorite presence or the diagenetic transformation of precursor components that were initially present in the primary sediment. A study of modern environments is thus an appropriate way of developing an understanding (by analogy) of the distribution of chlorite in sandstones, since the distribution of chlorite, or the key components of chlorite (Fe-oxides, Al-oxides and Si-oxides) in the original sediment, controls where chlorite will be found in the sandstone after burial diagenesis (Worden & Morad, 2003; Worden *et al.*, 2018). The first stages of sediment burial should however be considered carefully, since during this phase sediment may be part of an open-system. For example, widespread kaolinization has been

reported to be typical in marginal marine settings due to meteoric water-flushing; especially in lowstand system tract sandstones (Ketzer *et al.*, 2003). Consequently, clay mineral distribution patterns have been linked to sequence stratigraphy (Morad *et al.*, 2013). Furthermore, the co-deposition or diagenetic formation of other minerals may also inhibit or promote the development of authigenic chlorite. For example, iron is necessary for Fe-chlorite growth but may preferentially be locked up at the expense of chlorite by pyrite and siderite which tend to precipitate more quickly than Fe-silicates (Worden & Morad, 2003).

This study speculates that there are three discrete dominant controls on clay mineral distribution patterns in marginal marine settings, although note that all three may operate to different degrees at the same time. First, clay mineral distribution patterns may be controlled by provenance, and reflect the relative contribution of different potential sources of clay minerals (i.e. different bedrock types, drift deposits and offshore sediment). Second, hydrodynamic processes in the estuary may control the redistribution of clay minerals (possibly from one or multiple sources) and thus the relative abundance of a specific clay mineral may be associated with certain depositional environments. Third, there may be continued weathering and alteration of pre-existing clay minerals and/or sedimentary grains (for example, feldspars or lithics) in the estuary via a combination of physical, chemical and/or biological processes.

Estuarine clay mineral assemblages have been reported to be similar to those in the near-offshore (Postma, 1967; Meade, 1969; Hathaway, 1972), leading to a conclusion that landward displacement of marine sediment, during marine transgression, may explain some clay mineral distribution patterns (Chamley, 1989). It is noteworthy that, across the sediment below the world's ocean, clay minerals are not uniformly distributed. The type and relative abundance of clay minerals found in modern oceanic and marginal-marine settings has been reported to be governed primarily by a combination of climate (weathering intensity) and the type of sediment supplied (provenance) (Eberl *et al.*, 1984; Chamley, 1989; Rateev *et al.*, 2008). Chlorite and illite have been reported to be most abundant in high-latitude marine environments adjacent to land masses, subject to relatively cold climatic conditions that favour mechanical weathering (Windom, 1976; Eberl *et al.*, 1984; Chamley, 1989; Rateev *et al.*, 2008). Kaolinite has been reported to be most abundant in low-latitude marine environments adjacent to land masses with warm and humid conditions that permit intense chemical weathering (Windom, 1976; Eberl *et al.*, 1984; Chamley, 1989; Rateev *et al.*, 2008). Smectite is generally typical of weathering from semi-arid continental sources, subject to only the early stages of chemical weathering conditions (Salem *et al.*, 2000). It has been reported that provenance plays a critical role in determining the clay mineral assemblage in marginal marine settings (Chamley, 1989). For example, Rudert & Müller (1981) suggested that the relatively homogenous clay mineral assemblages reported within south-eastern estuaries from the North Sea, from Denmark (Varde Å) to The Netherlands (Rhine-Meuse), reflects the minor variability of north-western European climatic conditions and soil composition. In contrast, diverse estuarine clay mineral assemblages reported from British and North American estuaries was interpreted to reflect the heterogeneous composition of continental rocks and soils in the hinterlands of each estuary (Biddle & Miles, 1972; Hathaway, 1972).

Hydrodynamic processes in an estuary control the redistribution of the sediment fed into the estuary. The competing physical forces of inward river flow, wave energy transmitted from the open ocean and twice-daily tidal emptying and filling will combine to move sediment into specific sub-environments, such as salt marshes, mud flats, tidal bars, channels and the local foreshore (Dalrymple *et al.*, 1992).

Not all clay minerals necessarily have the same mean grain size, shape and/or density, so that different clay minerals may be preferentially associated with different sub-environments. It is also noteworthy that not all clay minerals are necessarily clay grade (clay minerals may be >2 μm in size); clay minerals may exist in lithic silt or sand grains, as discrete silt or sand grade grains, as well as in the finest grain-size fraction (clay grade) of any sediment. Once suspended, clays and clay minerals that have been fed into an estuary may undergo flocculation into larger aggregates, which subsequently preferentially settle out of the water column. Laboratory studies undertaken by Whitehouse *et al.* (1960) reported that, in relatively slow moving (or static) and brackish waters (1·8% salinity), kaolinite settles prior to illite. However Edzwald & O'Mella (1975) and Gibbs (1977) suggested that results from Whitehouse *et al.* (1960) have been wrongly extrapolated from the laboratory to the

natural environment. Edzwald & O'Mella (1975) instead suggested that suspended illite is more stable (slower aggregation or flocculation rate) than kaolinite, and thus should be deposited downstream relative to kaolinite. Conversely, Gibbs (1977) proposed that clay mineral distribution patterns are due to physical sorting by size, irrespective of mineralogy. It was suggested that mixing of fluvial and marine waters with distinctly different clay mineral suites, combined with estuarine circulation patterns, can explain clay mineral distribution patterns in the James River Estuary, Virginia, USA (Feuillet & Fleischer, 1980).

On top of provenance and hydrodynamic sorting controls on the proportions of clay minerals in marginal marine sediment, it has further been suggested that early diagenesis can alter the clay mineralogy of sediment in the environment very soon after deposition. It is possible that early diagenesis is simply a continuation of the physical and chemical alteration (weathering) processes that started in the hinterland and continued when the sediment was in transit. However, marginal marine, and especially estuarine, environments tend to be geochemically active given that they typically accumulate organic matter and contain sediment that is physically stable enough to develop active micro-biological and macro-biological communities (Berner & Berner, 2012).

Both physicochemical (Grim & Johns, 1954; Griffin & Ingram, 1955; Powers, 1957; Nelson, 1960; Daneshvar & Worden, 2018) and biologically-mediated (McIlroy *et al.*, 2003; Needham *et al.*, 2004; Worden *et al.*, 2006) early-diagenetic mineral alteration processes have been reported in deposited estuarine sediment. Large-scale studies of the Amazon River mouth concluded that rapid alteration of clay minerals and biogenic silica occurred in deltaic sediment (Michalopoulos & Aller, 1995, 2004; Aller & Michalopoulos, 1999; Michalopoulos *et al.*, 2000).

A detailed study of the clay mineralogy of a modern estuary was thus designed to establish whether clay mineral proportions are controlled by: (i) the distribution of various potential sources of clay minerals (ii) estuarine hydrodynamics and redistribution of material; and/or (iii) continued chemical and/or biological alteration of sedimentary minerals in the estuary. To achieve this, it is necessary to understand what clay minerals are being fed into the estuary from all of the various sources. It is also necessary to establish the average, or overall, clay mineral assemblage of the estuary and to determine how the clay minerals are distributed, if they are not homogenous. The Ravenglass Estuary, in north-west England

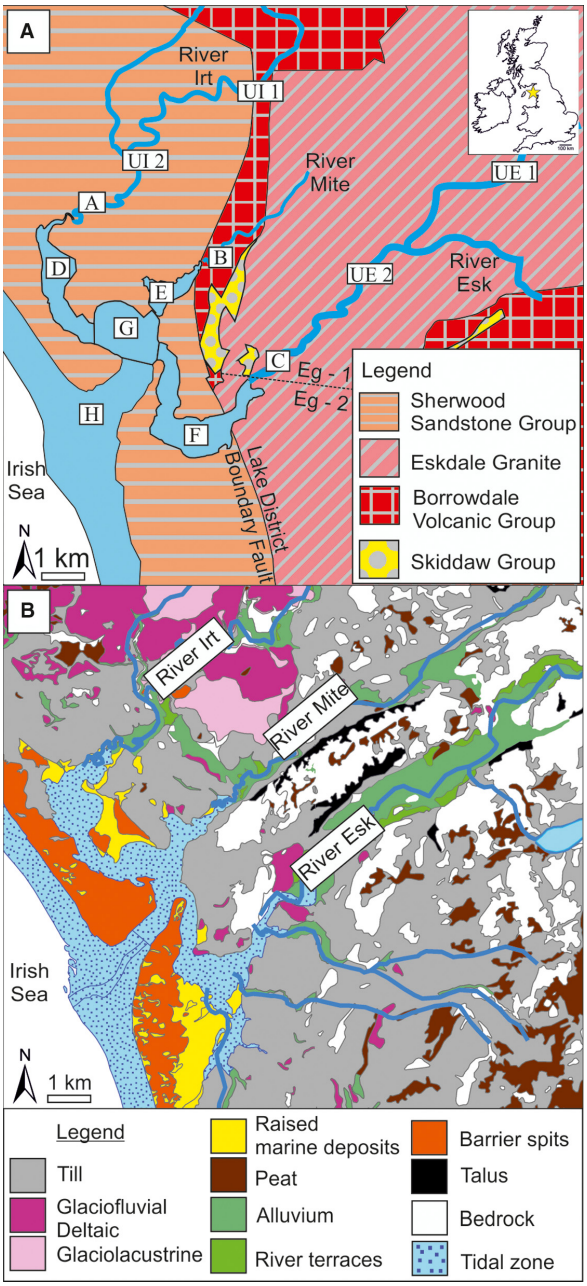

Fig. 1. Geological setting of the Ravenglass Estuary, UK. (A) Bedrock geology. Note that Eskdale Granite – 1 (Eg-1) and Eskdale Granite – 2 (Eg-2) are distinguished. (B) Quaternary drift-deposits. Upper-fluvial sediment sampling locations and estuarine zones are labelled accordingly; UI, upper-Irt; UE, upper-Esk; A, lower-Irt; B lower-Mite; C lower-Esk; D, inner-Irt; E, inner-Mite; F, inner, Esk; G, central-basin; and H, outer-estuary. Refer to Table 1 for mineralogical compositions of each geological unit.

(Fig. 1), has been selected for a high spatial resolution study of the surface (<2 cm) clay mineral distribution, along with a study of the clay mineralogy of the various provenance sources, followed by statistical analysis.

STUDY AREA: RAVENGLASS ESTUARY

The Ravenglass Estuary, in north-west England (Fig. 1), sits near the small town of Ravenglass located on the west coast of Cumbria. The Ravenglass Estuary, which encompasses the tidal reaches of the Rivers Esk, Irt and Mite, occupies an area of 5·6 km^2, of which *ca* 86% is intertidal (Bousher, 1999; Lloyd *et al.*, 2013; Wooldridge *et al.*, 2017a,b). It has been suggested (Bousher, 1999) that the Drigg and Eskmeals barrier-spits developed at around 3000 BP, causing the coalescence of the previously separate and westward flowing Rivers Irt, Mite and Esk, into a singular complex estuary with one main channel out to the Irish Sea. The estuary is macro-tidal (>7 m tidal range) and is fed by two dominant arms separated by Muncaster Fell (Fig. 2); the River Esk drains a southern hydrological basin and the River Irt drains a northern hydrological basin (Fig. 1). The Ravenglass Estuary is here thus defined as a 'dual-funnelled', mixed-energy estuary.

The northern part of the UK (including Cumbria) is presently undergoing limited isostatic recovery following the last glacial maximum (Bousher, 1999). The west Cumbria region of the UK was affected by glaciation during the Quaternary on at least three occasions. The last glaciation occurred in the late Devensian, at about 28 to 13 ka (Moseley, 1978; McDougall, 2001). The Ravenglass area has benefitted from substantial geological and geomorphological research due to the Sellafield nuclear reprocessing plant being 20 km north, and the low level nuclear waste repository at Drigg. Much of the glacial deposit has been removed from the land surface following the last glaciations (Merritt & Auton, 2000). The upper group of Quaternary sediments within the

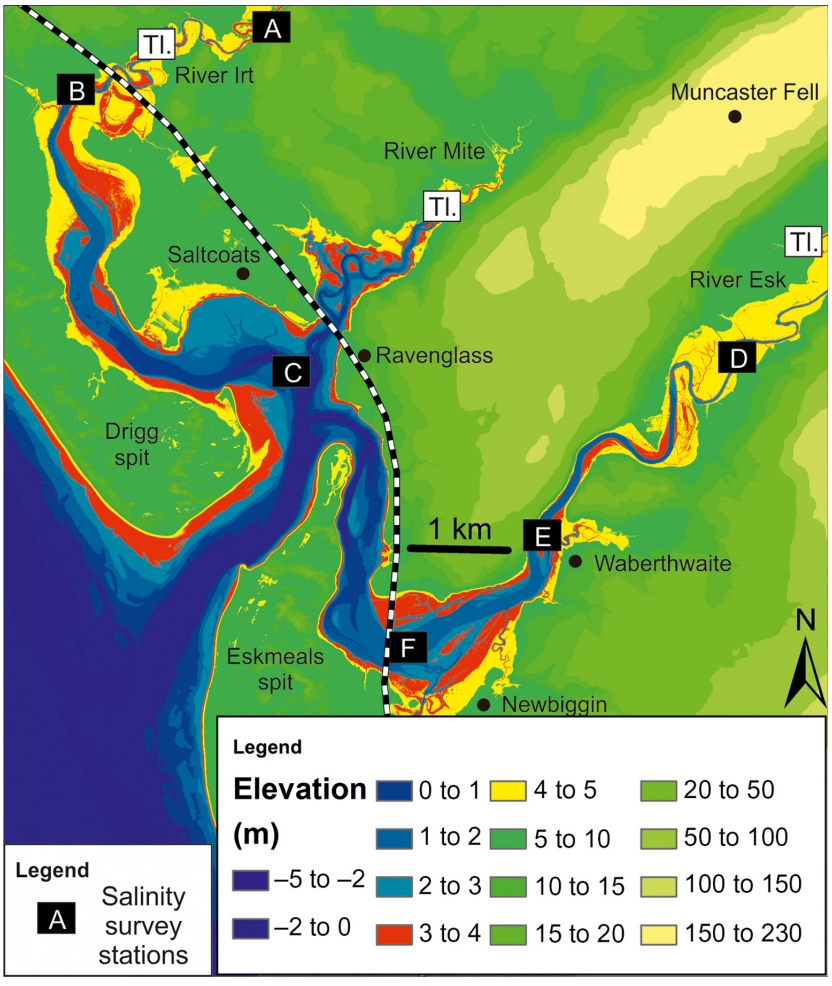

Fig. 2. Estuarine bathymetry and hinterland elevation (metres above Ordnance Datum) derived from Lidar Imagery. Stations in which salinity has previously been measured (Assinder *et al.*, 1985; Daneshvar, 2015) are labelled (A) to (F). Tidal limits are marked, after Kelly *et al.* (1991).

area around Sellafield and Ravenglass has been reported to include estuarine, alluvial, organic and aeolian sequences sitting on top of the final glacial deposits (Merritt & Auton, 2000). The estuarine sediments have a maximum thickness of about 10 to 15 m in this area (Bousher, 1999).

Geological setting and sediment source areas

The Rivers Irt, Mite and Esk drain a variety of bedrock lithologies and drift deposits (Fig. 1; Table 1). Upland catchment areas are composed of Devonian Eskdale Granite, Ordovician Borrowdale Volcanic Group and Cambrian Skiddaw Group rocks (Fig. 1A). These Palaeozoic rocks juxtapose the low lying coastal plains of the Triassic Sherwood Sandstone Group, with the Lake District Boundary Fault separating Palaeozoic from Mesozoic rocks. The Skiddaw Group includes weakly metamorphosed, fine-grained sedimentary rocks (Merritt & Auton, 2000). The Borrowdale Volcanic Group is dominated by subduction-related, K-rich, calc-alkaline andesite that forms the central component of the Lake District massif (Quirke *et al.*, 2015). The Borrowdale Volcanic Group was subject to regional, subgreenschist facies metamorphism at about 395 Ma, during the Caledonian Orogeny (Quirke *et al.*, 2015). The Eskdale Granite is part of the Lake District Batholith, at the western-margin of the Lake District massif; the southern part is granodioritic, while the northern part is coarse-grained granite (Young *et al.*, 1986). In both granite types, chloritisation of mafic silicates and plagioclase-alteration are widespread (Moseley, 1978; Young *et al.*, 1986; Quirke *et al.*, 2015). The Lower Triassic Sherwood Sandstone Group rocks are predominantly composed of fluviatile sandstones, locally known as the St Bees sandstone (Quirke *et al.*, 2015). The Ravenglass Estuary is thus predominantly fed by the southern River Esk, which drains an area dominated by Eskdale Granite, and the northern River Irt, which drains a combination of Borrowdale Volcanic Group andesites and Triassic Sherwood Sandstone Group sedimentary rocks.

Glacial till is exposed as knolls in all zones (inner, central and outer) within the estuary. These Quaternary sediments (Fig. 1B), in the Ravenglass Estuary area, contain distinctive clasts of the underlying bedrocks, allowing detailed lithostratigraphical division, as well as revealing complex ice-movement patterns (Merritt & Auton, 2000). Fluctuations in relative sea-level during the Holocene were caused by glacioeustatic sea-level change and spatially-variable glacioisostatic rebound following deglaciation. These sea-level fluctuations led to the deposition of a suite of tills, glaciofluvial and glaciolacustrine deposits (Fig. 1B), locally known as the Seascale Glacigenic Formation (predominantly the Ravenglass Till member) and the overlying Gosforth Glacigenic Formation (Merritt & Auton, 2000; Lloyd *et al.*, 2013).

Morphology and hydrodynamics

The geological and topographic constraints on the width of the arms of the estuary and gradients of the lower parts of the river catchments (Figs 1 and 2) constrain the area of the estuary to 5·6 km^2; this is typical of estuaries within north and western parts of the UK (Pye & Blott, 2014). Due to frictional effects commonly associated with shallow estuaries (Fig. 2), tidal cycles at Ravenglass are strongly asymmetrical, resulting in slightly prolonged, outward ebb tidal flows in comparison to the inward flood tidal flows (Kelly *et al.*, 1991). The rivers flowing into the estuary have average flow-rates of 3·4 $m^3\ sec^{-1}$ for the Irt, 4·2 $m^3\ sec^{-1}$ for the Esk and 0·4 $m^3\ sec^{-1}$ for the Mite (Bousher, 1999). The maximum discharge measured for the lower Esk arm of the estuary during the ebb is only slightly lower at 4·99 $m^3\ sec^{-1}$ than the flood at 5·41 $m^3\ sec^{-1}$; interpreted to result from quick-ebb drainage due to the estuary being short in length (Kelly *et al.*, 1991).

Longitudinal salinity gradients (from the tidal limit to the open-sea) reported by Assinder *et al.* (1985) & Daneshvar (2015) and are shown in Fig. 2. Stations A and D are reported as freshwater (Assinder *et al.*, 1985; Daneshvar, 2015). Water-sampling stations B (River Irt) and E (River Esk) were reported to be freshwater-dominated, with only minor marine dilution of the freshwater, creating brackish-water conditions for *ca* 2·5 h at high-tide (Assinder *et al.*, 1985; Daneshvar, 2015). Water-sampling stations C (Saltcoats) and F (River Esk bridge viaduct) were reported to be seawater-dominated (i.e. approaching seawater salinity), with only minor freshwater incursions during low-tide (Assinder *et al.*, 1985; Daneshvar, 2015).

Anthropogenic impact on the estuary is here considered to be minor since the surrounding area is sparsely populated, although the construction of the railway bridge has resulted in constriction and sheltering of the River Mite (Fig. 2). Cartographic evidence also suggests that fringing salt marsh has at least partially

Table 1. Mineralogical descriptions of hinterland bedrock and drift deposits.

Lithology	Mineralogical description
Fishgarth Wood Till Member (part of the Gosforth Glaciogenic Formation)	Holocene glacial till. The matrix-supported sandy–silty–clay diamicton also includes clasts of Borrowdale Volcanic Group lithologies, granite, granophyre, olive brown siltstone and sandstone (Merritt & Auton, 2000)
Ravenglass Till (part of the Seaforth Glaciogenic Formation)	Holocene glacial till. Dispersed clasts (up to boulder size) of Borrowdale Volcanic Group lithologies, granite, granophyre, siltstones, with minor concentrations of sandstones, ironstones and shell fragments are present (Merritt & Auton, 2000)
St. Bees Sandstone (part of the Sherwood Sandstone Group)	Lower Triassic sandstone. Feldspathic or subarkosic, with dominant quartz and K-feldspar, albite, muscovite, biotite grains and minor Fe oxides (Quirke *et al.*, 2015). Borrowdale Volcanic Group lithic fragments occur towards the base of the formation (Strong *et al.*, 1994). Diagenetic phases include dolomite, quartz overgrowths and calcite authigenesis (Strong *et al.*, 1994)
Eskdale Granite – 1	Coarse-grained Devonian granite. Typical for the Eskdale Granite, plagioclase feldspars are more altered than K-feldspars (Simpson, 1934). Plagioclase phenocrysts have relatively unaltered Na-rich rims with pervasively altered cores, forming fine-grained aluminous clay mineral alteration products (Quirke *et al.*, 2015). Biotite crystals with incipient alteration to chlorite (Fe/Mg 2·5) are abundant. Opaque Fe-oxides (predominantly ilmenite) occur as inclusions within the main silicates as well as groundmass phases, and as <0·15 mm grains (Quirke *et al.*, 2015)
Eskdale Granite – 2	Devonian granodiorite. Both plagioclase and K-feldspars are more altered than those found within Eskdale granite – 1. Micas are Fe-rich and Al-poor, and classified as phengite. Intergrowths of white-mica and relatively Mg-enriched chlorite (Fe/Mg 0·6) are reportedly pseudomorphs after biotite or hornblende (Simpson, 1934; Quirke *et al.*, 2015)
Borrowdale Volcanic Group	Ordovician andesitic extrusive igneous rocks. Fine-grained groundmass shows ophitic textures between euhedral altered plagioclase and K-feldspar and patchy chlorite or biotite. Primary plagioclase phenocrysts have been partly altered to muscovite. Relatively Fe-enriched chlorite (Fe/Mg 1·8) crystals (*ca* 1 mm diameter) are reported to be pseudomorphs after pyroxene (Quirke *et al.*, 2015)
Skiddaw Group	Cambrian metamorphic rocks. Lower grade rocks are reported to be dominated by illite, chlorite and interlayered illite-smectite, whereas the higher grade rocks are dominated by muscovite and chlorite, and commonly interlayered paragonite–muscovite (Young *et al.*, 1986). Aluminous K-mica with low phengite content dominates the rock and are characteristic of the Skiddaw Group (Stone & Merriman, 2004)

developed as a consequence of the railway viaduct construction (Carr & Blackley, 1986).

The Ravenglass Estuary has been divided into zones, which may be grouped into four categories (Fig. 1A), based upon the dominant physical processes active in each zone: (i) fluvial (river) zone, freshwater-dominated in the Esk (zone A), Mite (zone B) and the Irt (zone C); (ii) a brackish, inner river-dominated and tide-dominated Irt, (zone D), Mite (zone E), and Esk (zone F); (iii) a relatively mixed-energy (fluvial, tide and wave-influenced), heterogeneous central zone (zone G) with near-seawater salinity, which contains extensive mud-flat and mixed-flat (Saltcoats tidal flat); and (iv) an outer zone (zone H), dominated by seawater with wave and/or tidal currents, which are dissipated by barrier-spits.

SAMPLES AND METHODS

In order to study the clay mineral distribution, it was necessary to determine the surface sedimentology by defining all depositional environments throughout the estuary, describing surface sediment characteristics, collecting samples and then analysing them by X-ray diffraction (XRD)

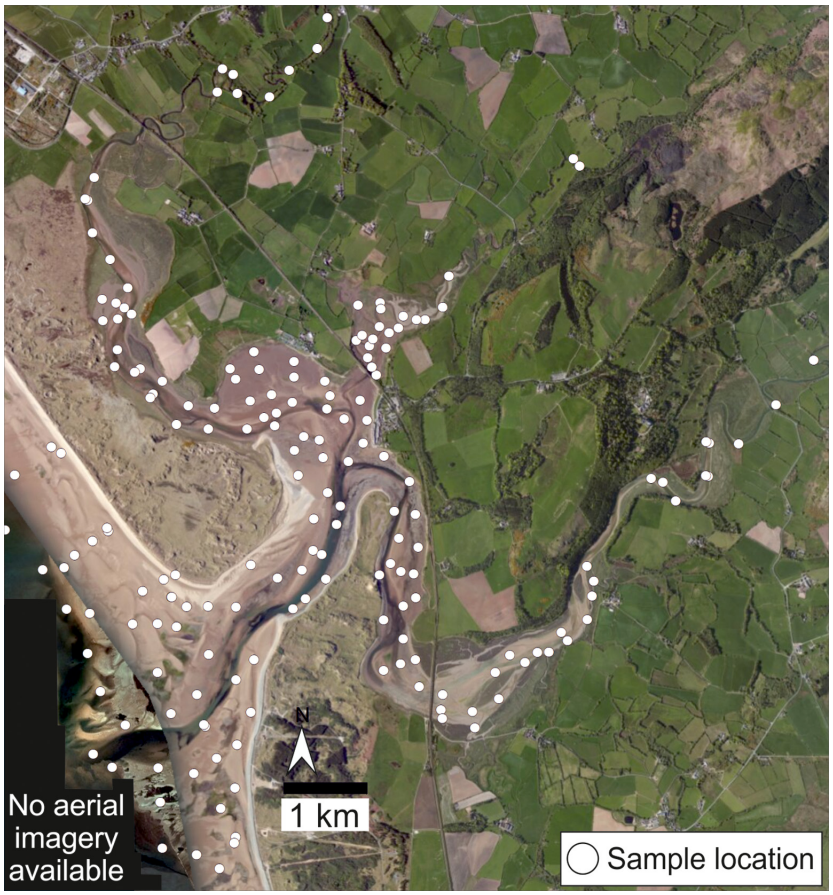

Fig. 3. Distribution of surface (<2 cm below the sediment surface) samples used for X-ray diffraction (XRD) and Laser Particle Size Analyses (LPSA) (n = 206).

preceded by sample separation into different grain size fractions.

Field mapping and sample collection

Aerial photographs (Fig. 3) and detailed ground surveys were used to define a suite of sub-environments: gravel-bed; tidal flats, tidal bars and dunes; tidal-inlet; backshore; foreshore; and pro-ebb delta. Tidal-flats have been further subdivided and categorised based on the percentage of sand; calculated using subsequent Laser Particle Size Analysis (LPSA) of surface sediment samples (Fig. 3) (see later in this section). The tidal-flat classification scheme of Brockamp & Zuther (2004) was employed, whereby a sand-flat is >90 sand, a mixed-flat has 50 to 90% sand, and a mud-flat has 15 to 50% sand.

Sediment for laboratory analysis was collected at low-tide along pre-defined transects at 185 sites in order to give an approximately uniform distribution of samples (Fig. 3). Sediment was also collected from 21 fluvial sample locations; four upper fluvial samples are marked on Fig. 1. All sediment samples were placed in air-tight, screw-top, plastic jars in the field before storing them in a refrigeration unit at *ca* 2°C. This procedure prevented sample degradation prior to LPSA and XRD analyses.

Grain size and sorting were determined for all collected sediment samples by LPSA analyses using a Beckman Coulter Laser Particle Size Analyser (Beckman Coulter Life Sciences, Indianapolis, IN, USA), in unison with GRADISTAT (Blott & Pye, 2001). This revealed the mean grain size, grain-size sorting and sand percentage at 206 surface sediment sites (Fig. 3). This paper uses the grain-size sorting (σg) scale presented by Folk & Ward (1957), where high-values are indicative of poorly-sorted sediment. Additionally, in order to characterise the whole estuary at high resolution, surface sediment grain size was determined with a hand-lens at 3151 sites across the estuary using a grain-size comparison card.

In order to assess the macrobiological activity in the sediment throughout the estuary, the abundance of *Arenicola marina* (lugworms) was

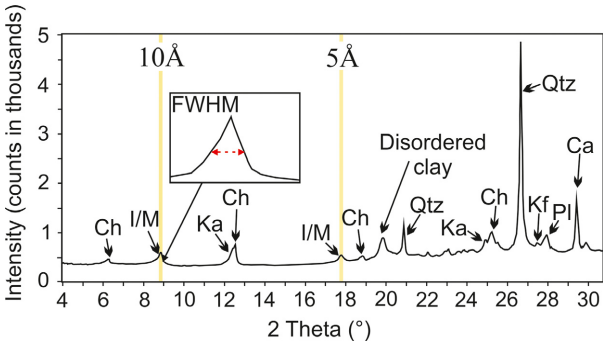

Fig. 4. Example X-ray diffractogram used to quantity clay mineral abundance. Illite crystallinity is measured on the 10Å illite peak, using the full width at half maximum (FWHM, full width at half-maximum). Esquevin Index is derived by comparing the relative peak heights of the 5Å and 10Å illite peaks. The abbreviations for specific minerals are as follows; Ch, chlorite; I/M, illitic material including clay-size micaceous material, here termed illite; Ka, kaolinite; Qtz, quartz; Kf, K-feldspar; Pl, plagioclase; and Ca, calcite.

determined at 3182 sites by counting the number of *Arenicola marina* faecal castings per square metre, using a 1 m^2 quadrat. The quadrat was thrown randomly, i.e. blindly thrown behind the individual doing the measurement, to ensure an absence of bias.

Clay mineral separation, identification and quantification

Surface-sediment clay fractions (<2 μm) from the estuary were determined by physical separation prior to XRD analysis. Samples were physically separated in an ultrasonic bath, followed by centrifuge settling at 5000 rpm for 10 min to isolate the clay fraction (<2 μm). The wet-separated clay fractions were then dried at 60°C for 24 h and weighed to calculate the percentage of clay-size material within each surface sample.

The clay mineralogy of all the estuary samples was determined by X-ray diffraction analysis of randomly-orientated powders using a PANalytical X'Pert Pro MPD X-ray diffractometer (Malvern PANalytical, Malvern, UK; Fig. 4). Randomly-orientated powders, as opposed to orientated mounts, were chosen to achieve the precise (repeatable) quantification of all clay minerals. The minerals were quantified using the relative intensity ration (RIR) method proposed by Chung (1974a) and (Chung, 1974b) using PANalytical HighScore Plus software. To assess the presence of expandable clay minerals, samples were glycolated for 24 h and re-scanned over a range of 3·9 to 13·0°2θ (Moore & Reynolds, 1997).

An array of grain-size separates; <0·2 μm (fine clay); 0·2 to 2·0 μm (coarse clay); 2 to 32 μm (fine silt); 32 to 63 μm (coarse silt); 63 to 125 μm (fine sand); and 125 to 250 μm (medium sand), using a combination of gravity-settling (as above) and sieving, was used to reveal the X-ray diffraction mineralogy of different size-fraction separates. Relative abundances of chlorite (chlorite/(chlorite + illite + kaolinite)), kaolinite (kaolinite/(chlorite + illite + kaolinite)), and illite (illite/(chlorite + illite + kaolinite)) were derived to assess the relative abundance of each clay mineral at each sample location.

In this study, the term *illite* is used for the clay-size, mica-like minerals (10Å non-expandable clay) commonly associated with argillaceous sediments, following the definition of Grim *et al.* (1937); also termed *illitic material* (Moore & Reynolds, 1997). Furthermore, Esquevin Indices and illite crystallinity were calculated in an attempt to differentiate illite types in the Ravenglass Estuary, based upon composition and crystallinity.

The Esquevin Index (revealing illite chemistry) has been calculated by analysing the ratio between the intensity of the 5Å and 10Å peaks i.e. the ratio between the (002) and (001) peak heights (Esquevin, 1969), on X-ray diffractograms (Fig. 4). High Esquevin Indices indicate Al-rich illites (with muscovite representing the highest Esquevin Index end-member), reported to correspond to chemically-weathered rocks that have lost divalent cations (Fe and Mg) from the octahedral sites (Chamley, 1989). In contrast, low Esquevin Indices represent relatively Fe–Mg-rich illite (with biotite representing the lowest Esquevin Index end-member), which is considered to be characteristic of physically eroded, unweathered rocks (Chamley, 1989). The following classification boundaries have here been used, after Esquevin (1969); biotite, <0·15; biotite + muscovite, 0·15 to 0·3; phengite, 0·3 to 0·4; muscovite, >0·4.

The illite crystallinity index ($2^{O}\theta$), also known as the Kübler Index (Kübler, 1964), was determined by measuring the full width at half-maximum peak height (FWHM) of the 10Å (001) illite peak on X-ray diffractograms (Fig. 4). Illite crystallinity is inversely proportional to the temperature at which the illite formed: low illite-crystallinity indices (low FWHM, narrow basal-reflections) indicate highly crystalline, relatively unaltered, high growth temperature, high-structural-order illite; whereas high illite-crystallinity values (high FWHM, broad basal reflections) indicate poorly-

crystalline, highly-degraded, low growth temperature, low-structural-order illite (Kübler, 1964; Chamley, 1989). The following boundaries are used here, after Kübler (1964); epizone (highest temperature): <0·25; anchizone: 0·25 to 0·42, diagenesis (lowest temperature): >0·42. When used in provenance studies (Gingele *et al.*, 2001; Oliveira *et al.*, 2002; Borchers *et al.*, 2011; Bout-Roumazeilles *et al.*, 2013; Du Chatelet *et al.*, 2016), a key assumption typically employed is that illite crystallinity remains unchanged between supply, transport and deposition, i.e. there is no subsequent alteration of illite crystallinity or chemistry within the sedimentary environment.

Bedrock and drift analyses

In order to compare estuary sediment to the drift deposits (Fig. 1B), clay fractions (<2 μm) from both the Seascale and the Gosforth Glacigenic Formations were determined by physical separation prior to XRD analysis. Samples were physically separated in an ultrasonic bath, followed by centrifuge settling at 5000 rpm for 10 min to isolate the clay fraction. The wet-separated clay fractions were then dried at 60°C for 24 h and weighed to calculate the percentage of clay-size material within each surface drift sample. All drift samples were then analysed by PANalytical X'Pert Pro MPD X-ray diffractometer using the same approaches as listed for the estuary sediment samples.

Although substantial work has been previously undertaken for the bedrock in the hydrological basins that supply the Ravenglass Estuary, several samples of the Triassic Sherwood Sandstone, Borrowdale Volcanic Group and Eskdale Granite were collected, in order to allow for mineralogical analysis and direct comparison with the clay minerals in the estuary sediment samples. Samples of Sherwood Sandstone from St Bees Head, Eskdale Granite from Devoke Water and Borrowdale Volcanic Group from just west of Lake Wastwater, were all treated to produce clay mineral separates that are comparable to the modern sediment samples. Fresh, unweathered rock sub-samples were collected at each site using a hammer and chisel. Loose material was removed from the sub-sample using mild detergent and tap water before being dried at 60°C. A steel disc mill was used for 2 sec to crush the subsample to <1 mm particle sizes. A representative 5 g subsample was taken from the part-crushed material, and placed in an agate McCrone mill with 12 ml of distilled water and finely crushed for 10 min. The resultant slurry was washed into a petri dish using distilled water, and then dried at 60°C. The dried material was crushed into a fine loose powder using an agate pestle and mortar ready for XRD analysis using the same approaches as listed for the estuary sediment samples.

Spatial mapping and statistical analysis

All spatial distribution maps were made in ArcGIS using an inverse distance weighted (IDW) interpolation technique, in order to avoid the creation of ridges or valleys of extreme and unrepresentative values (Watson & Philip, 1985). The insertion of an interpolation barrier, using a polyline drawn through the long axis of Drigg and Eskmeals spits, ensured interpolated values, on either side of the spits (i.e. in the estuary and on the coast), did not influence one another, despite their relative spatial proximity. Spatial maps have been plotted using a geometrical class-interval, in order to avoid divorcing the statistical distribution of data from its geographic context.

Pearson's correlation coefficients were calculated to describe the strength of the relationship between relative clay mineral abundance and host-sediment properties (mean grain size, grain size sorting, clay fraction, sand percentage and bioturbation intensity), as well as elevation (m OD). Statistical significance is highlighted using the following symbols; marginally significant (†) when $P < 0{\cdot}1$, significant (*) when $P < 0{\cdot}05$, very significant (**) when $P < 0{\cdot}01$, extremely significant (***) when $P < 0{\cdot}001$. An Analysis Of Variance (ANOVA) approach was used to assess whether there is a statistical difference ($P < 0{\cdot}05$) in relative clay mineral abundance (chlorite, kaolinite and illite) and illite type and illite crystallinity (Esquevin Index and FWHM) between estuarine zones (fluvial, inner, central and outer), as well as depositional environments (De1 to De9). Following ANOVA, post-hoc Tukey's honestly significant difference (HSD) test was employed to highlight where the identified significant differences in relative abundance could be found. All statistical analyses were performed in R statistical software (R Core Team, 2016).

RESULTS

The output of the surveys of surface characteristics, grain size, grain size sorting, abundance of clay fraction and lugworm density, together with

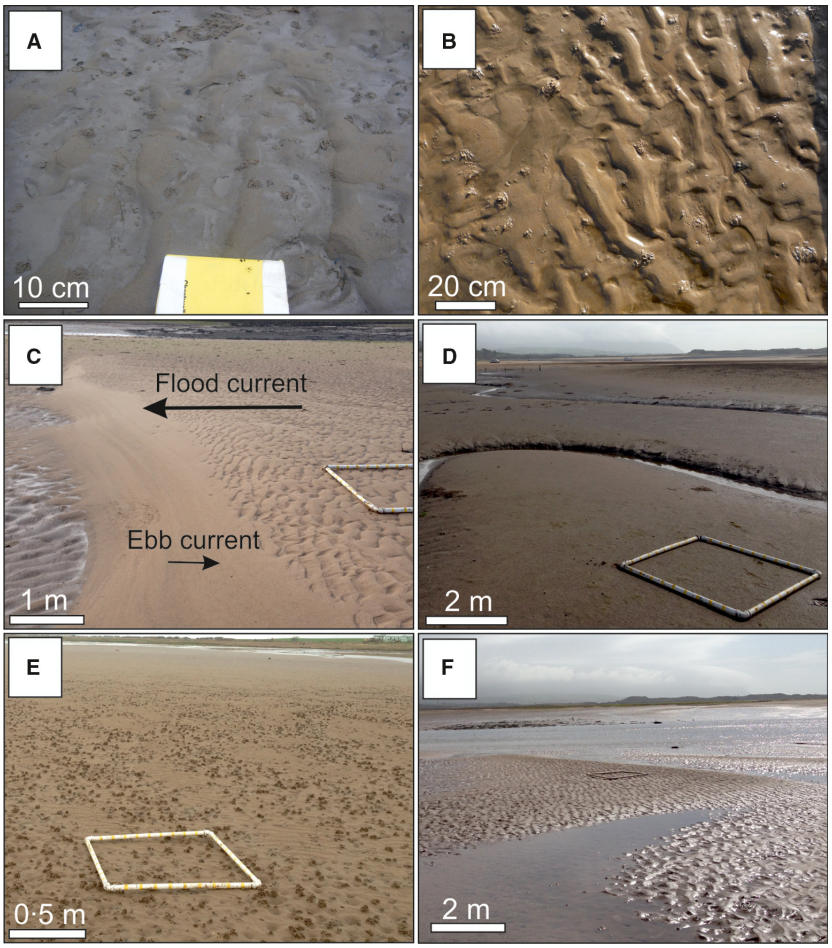

Fig. 5. Compilation of surface photographs taken throughout the Ravenglass Estuary: (A) and (B) inner estuarine sand-flats with mud-drapes; (C) inner estuary flood-dominated tidal-bar; (D) central basin mud-flat; and (E) central basin, highly-bioturbated (*Arenicola Marina*), mixed-flat; (F) central-basin low amplitude dunes. Note the white quadrat used to quantify lugworm (*Arenicola marina*) bioturbation intensity (castings per 1 m^2).

the X-ray diffraction results of the analysis of estuary sediment, fluvial sediment, drift deposits and bed rock samples will be presented here.

Estuary sediment characteristics

During the detailed field studies, nine discrete depositional environments were defined: gravel-beds (De 1), tidal flats (De2 to De4), tidal bars and dunes (De5), tidal-inlet deposits (De6), back-shore deposits (De7), foreshore deposits (De8) and pro-ebb delta deposits (De9). The tidal flats were subdivided into: mud-flats (De2); mixed-flats (De3); and sand-flats (De4) using subsequent LPSA analysis and the Brockamp & Zuther (2004) method of classification. The general appearance of the nine depositional environments is illustrated in Figs 5 and 6. The mapped distribution of the nine discrete depositional environments in the Ravenglass Estuary is displayed in Fig. 7. The average characteristics of the nine depositional environments, in terms of grain size, grain-size sorting, clay fraction and degree of lugworm bioturbation, are presented in Table 2. The estuary has also been subdivided into discrete zones (Fig. 1). The average characteristics of the eight estuary zones, in terms of grain size, grain sorting, clay fraction and degree of lugworm bioturbation, are presented in Table 3. The following text describes the appearance and character of the various depositional environments in the defined estuary zones.

The mapped distribution of grain size, grain sorting, clay fraction and degree of lugworm bioturbation, are presented Fig. 8. Grain size, grain-size sorting and the abundance of clay fraction as a function of depositional environment and estuarine zone are represented in Fig. 9.

Inner and central estuarine zones (zones D to G on Fig. 1A) are fringed by upper-tier, well-vegetated salt marsh, which transitions into moderately to sparsely vegetated and intensely bioturbated (*Corophium volutator*, also known as

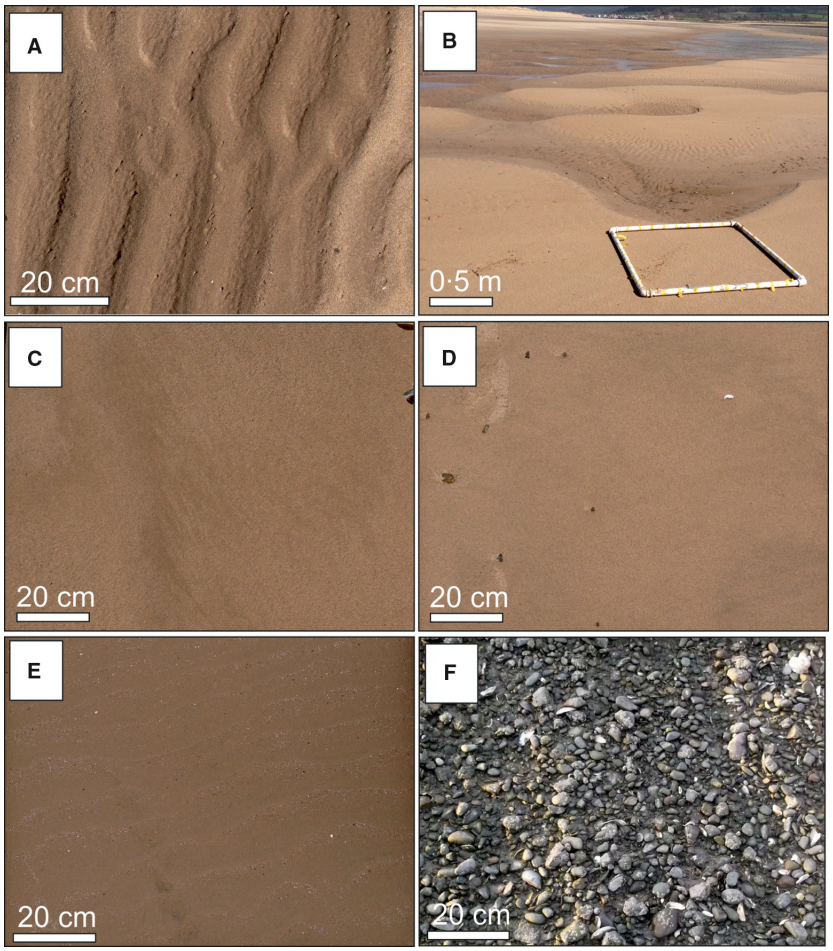

Fig. 6. Compilation of surface photographs taken throughout the Ravenglass Estuary: (A) upper-foreshore and tidal inlet wave-formed ripples; (B) tidal inlet, migratory three-dimensional dunes; (C) tidal inlet upper-phase plane bed, proximal to the ebb-channel; (D) wind-blown, upper foreshore sediment; (E) lower foreshore wave-formed ripples with subtle shell-debris lag deposits; and (F) gravel-bed, exposed in the inner Esk. Note, the white quadrat used to quantify lugworm (*Arenicola marina*) bioturbation intensity (castings per 1 m^2).

sand shrimp, which form <5 cm deep U-shaped burrows) middle-tier and lower-tier salt marsh (Fig. 7). Salt marsh grades into poorly-sorted (2·0 to 4·0 σg) clay-dominated and silt-dominated (<62 μm) mud-flats (Fig. 5D; Table 2), which are densely bioturbated by *Corophium volutator* but have a relatively sparse lugworm population (Fig. 8D).

Mud flats (Fig. 5D) within the inner and central (zones D to G on Fig. 1A) grade into poorly-sorted (2·0 to 4·0 σg) and very fine-grained (62 to 125 μm) mixed-flats (Figs 5E, 8 and 9; Table 2). Mixed-flats are highly-heterogeneous; substrates vary between lower-plane beds (including fluidised mud and sand) and sinuous to linguoid current ripples, typically draped in mud; bioturbation intensity (*Arenicola marina)* ranges from 0 to 115 castings per square metre (Fig. 8D), with a mean of four castings per square metre (Table 2). The inner and central zones have a wide range of mean grain size and grain sorting values (Fig. 9; Table 2).

In proximity to the ebb-channel, within the inner and central estuary (zones D to G on Fig. 1A), there is a gradational change from mixed-flats to moderately well-sorted to moderately sorted (1·41 to 2·00 σg) fine to medium-grained (125 to 350 μm) sand flats with sinuous to linguoid current ripples; mud-drapes are common (Figs 6A, 6B, 7 and 8). *Arenicola marina* is the dominant macrofauna in intertidal sand flats, with highly variable bioturbation intensity ranging from 0 to 48 castings per square metre (Fig. 8D), with a mean of about seven castings per square metre (Table 2). The lower inner Esk Estuary (zone F on Fig. 1) hosts gravel beds (Fig. 6F; partly colonised by mussels) which extend between the railway crossing and Ravenglass village (Fig. 7), directly adjacent to glacial till deposits.

Fine to medium grained (125 to 350 μm) and moderately well-sorted to moderately sorted (1·41 to 2·00 σg) tidal-dunes (in both the inner and central estuary; zones D to G on Fig. 1A) and tidal-

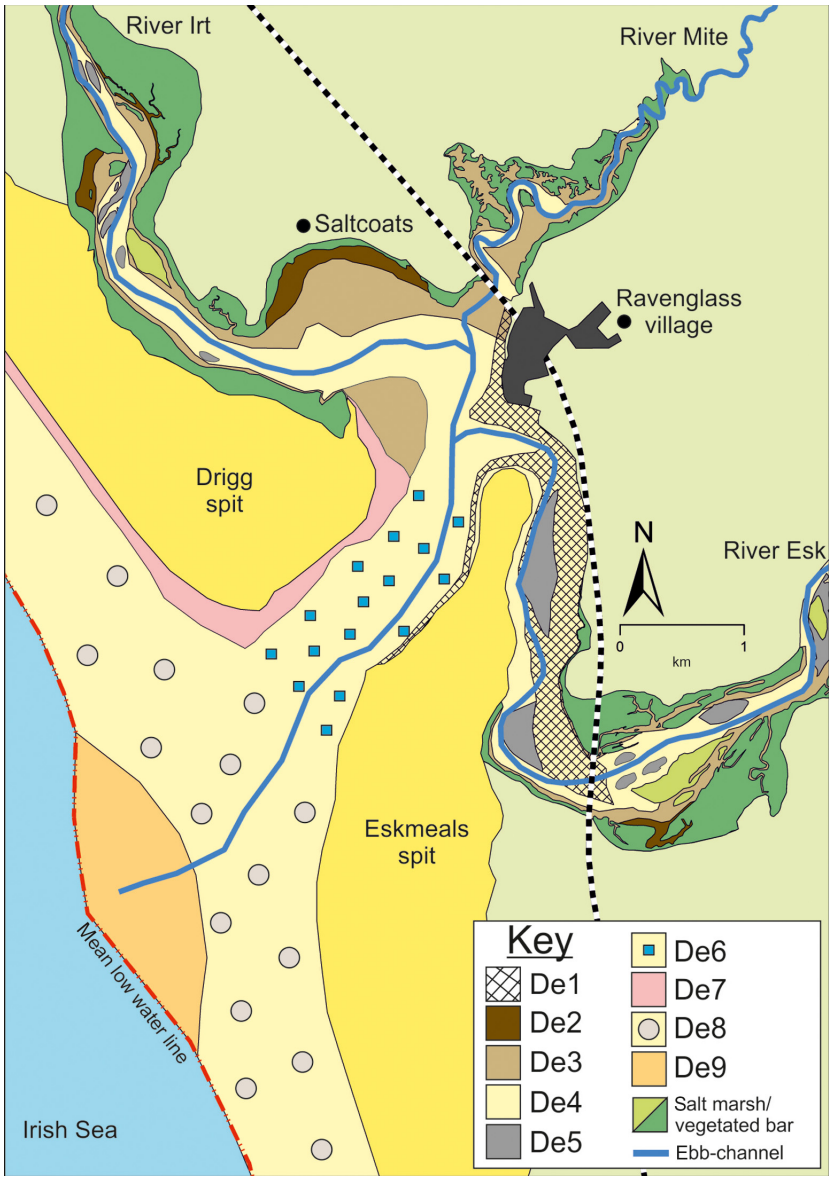

Fig. 7. Distribution of estuarine depositional environments within the Ravenglass Estuary. Depositional environments are labelled accordingly: De1, gravel-bed; De2, mud-flat; De3, mixed-flat; De4, sand-flat; De5, tidal bars and dunes; De6, tidal-inlet; De7, backshore; De8, foreshore; and De9, pro-ebb delta.

bars (inner estuary only; zones D to F on Fig. 1A), generated by flood tidal-currents, are proximal to the channel-axis (Fig. 5C and F; Table 2). Bioturbation intensity (*Arenicola marina)* is relatively low and ranges from zero to eight castings per square metre (Fig. 8D), with a mean of about one casting per square metre (Table 2). The transition from mixed-flat to sand-flat in the central basin (zone G on Fig. 1A) broadly reflects elevation; sand flats are typically <2 m OD (Fig. 2).

The outer estuary (zone H on Fig. 1A) is comprised of the tidal inlet (De6: the narrow-inlet that dissects Eskmeals and Drigg barrier-spits), foreshore (De8: defined as the section of beach between the backshore and the mean-low-water line) and backshore deposits (De7: tidally-inundated only during spring-tide and storm-events) (Fig. 7). Bioturbation is typically absent in the outer estuary (Table 2) with the exception of isolated patches in the tidal inlet (Fig. 8D; Table 2). The abundance of clay fraction in the outer estuary (Fig 8C; Table 2) is minor (<0·5%). Tidal inlet sediment is typically moderately well-sorted (1·41 to 1·62 σg) and medium-grained (250 to 500 μm). Wind-blown sands (backshore deposits) grade into tidal inlet substrates which contain both wave-ripples, three-dimensional dunes and, with increasing proximity to the ebb-channel, upper-phase plane beds (Figs 6, 7 and 8). Sediments upon the southern foreshore and in pro-ebb delta deposits

Table 2. Summary of the main characteristics of the nine depositional environments and their clay mineralogy attributes.

Depositional environment (code)	*n*	Mean grain size (mm)	Grain size sorting (σg)	Clay fraction (%)	Mean bioturbation (casts per m^2)	Illite index	SD	Chlorite index	SD	Kaolinite index	SD	Esquevin index (5Å/10Å)	SD	Illite crystallinity (FWHM)	SD
De1	10	371	1·86	0·99	1·30	0·607	0·012	0·180	0·009	0·213	0·006	0·28	0·02	0·25	0·02
De2	13	39	3·54	9·47	0·46	0·614	0·014	0·178	0·008	0·208	0·009	0·28	0·02	0·23	0·02
De3	44	115	2·37	5·05	4·07	0·607	0·015	0·183	0·008	0·210	0·012	0·29	0·03	0·24	0·02
De4	23	253	1·59	0·83	6·57	0·600	0·031	0·186	0·018	0·214	0·018	0·31	0·04	0·26	0·02
De5	14	283	1·59	1·08	1·14	0·596	0·023	0·185	0·013	0·220	0·015	0·32	0·04	0·27	0·03
De6	12	312	1·53	0·58	2·17	0·593	0·022	0·201	0·018	0·206	0·015	0·31	0·03	0·27	0·03
De7	4	324	1·36	0·08	0·00	0·564	0·025	0·234	0·013	0·202	0·014	0·35	0·03	0·27	0·03
De8	41	291	1·44	0·13	0·27	0·600	0·027	0·202	0·016	0·199	0·020	0·34	0·04	0·30	0·04
De9	10	239	1·48	0·12	0·10	0·613	0·021	0·188	0·017	0·200	0·011	0·34	0·04	0·29	0·05
Weighted average		225	1·90	2·36	2·36	0·602	–	0·190	–	0·208	–	0·31	–	0·27	–

Depositional environments are labelled accordingly: De1, gravel-bed; De2, mud-flat; De3, mixed-flat; De4, sand-flat; De5, tidal bars and dunes; De6, tidal-inlet; De7, backshore; De8, foreshore; and De9, pro-ebb delta. A weighted average ensures that densely sampled depositional environments (for example, n = 41 for De8) do not bias the average for a given variable (for example, mean grain size) across all depositional environments. Weighted averages are calculated by adding together the sum total of the average of a given variable (for example, mean grain size of 371 μm) multiplied by the number of samples analysed per depositional environment (for example, 10 for De1) divided by the total number of samples analysed across all depositional environments (i.e. n = 171). FWHM, full width at half-maximum.

Table 3. Summary of the main characteristics of the eight defined estuary zones and their clay mineralogy attributes.

Estuary zone	*n*	Mean grain size (mm)	Grain size sorting (σg)	Clay fraction (%)	Mean bioturbation (casts per m^2)	Illite index	SD	Chlorite index	SD	Kaolinite index	SD	Esquevin index (5Å/10Å)	SD	Illite crystallinity (FWHM)	SD
A	11	190	2·53	3·44	0·00	0·537	0·052	0·211	0·022	0·252	0·031	0·35	0·08	0·22	0·02
B	2	539	1·53	0·29	0·00	0·500	0·020	0·208	0·011	0·291	0·008	0·29	0·01	0·24	0·08
C	10	213	2·79	6·76	0·00	0·589	0·036	0·193	0·023	0·218	0·016	0·29	0·02	0·23	0·02
D	19	202	2·30	3·85	0·32	0·602	0·024	0·183	0·014	0·215	0·013	0·29	0·03	0·25	0·02
E	19	90	2·47	6·74	0·26	0·615	0·014	0·180	0·007	0·205	0·010	0·29	0·02	0·23	0·02
F	37	222	1·86	2·41	2·35	0·605	0·019	0·183	0·011	0·212	0·012	0·30	0·04	0·26	0·03
G	35	184	2·31	3·13	9·79	0·602	0·022	0·184	0·012	0·215	0·015	0·31	0·03	0·25	0·03
H	75	291	1·45	0·19	0·56	0·594	0·029	0·204	0·020	0·202	0·018	0·33	0·04	0·29	0·04
Weighted average		228	1·96	2·50	2·32	0·596	–	0·192	–	0·212	–	0·31	–	0·26	–

Estuarine zones are labelled accordingly: A, lower-Irt; B, lower-Mite; C, lower-Esk; D, inner-Irt; E, inner-Mite; F, inner, Esk; G, central-basin; and H, outer-estuary. A weighted average ensures that densely sampled estuarine zones (for example, n = 37 for zone F) do not bias the average for a given variable (for example, mean grain size) across all estuarine zones. Weighted averages are calculated by adding together the sum total of the average of a given variable (for example, mean grain size of 371 μm) multiplied by the number of samples analysed per estuarine zone (for example, 11 for zone A) divided by the total number of samples analysed across all estuarine zones (i.e. n = 208). Estuarine zones are shown in map form on Fig. 1A. FWHM, full width at half-maximum.

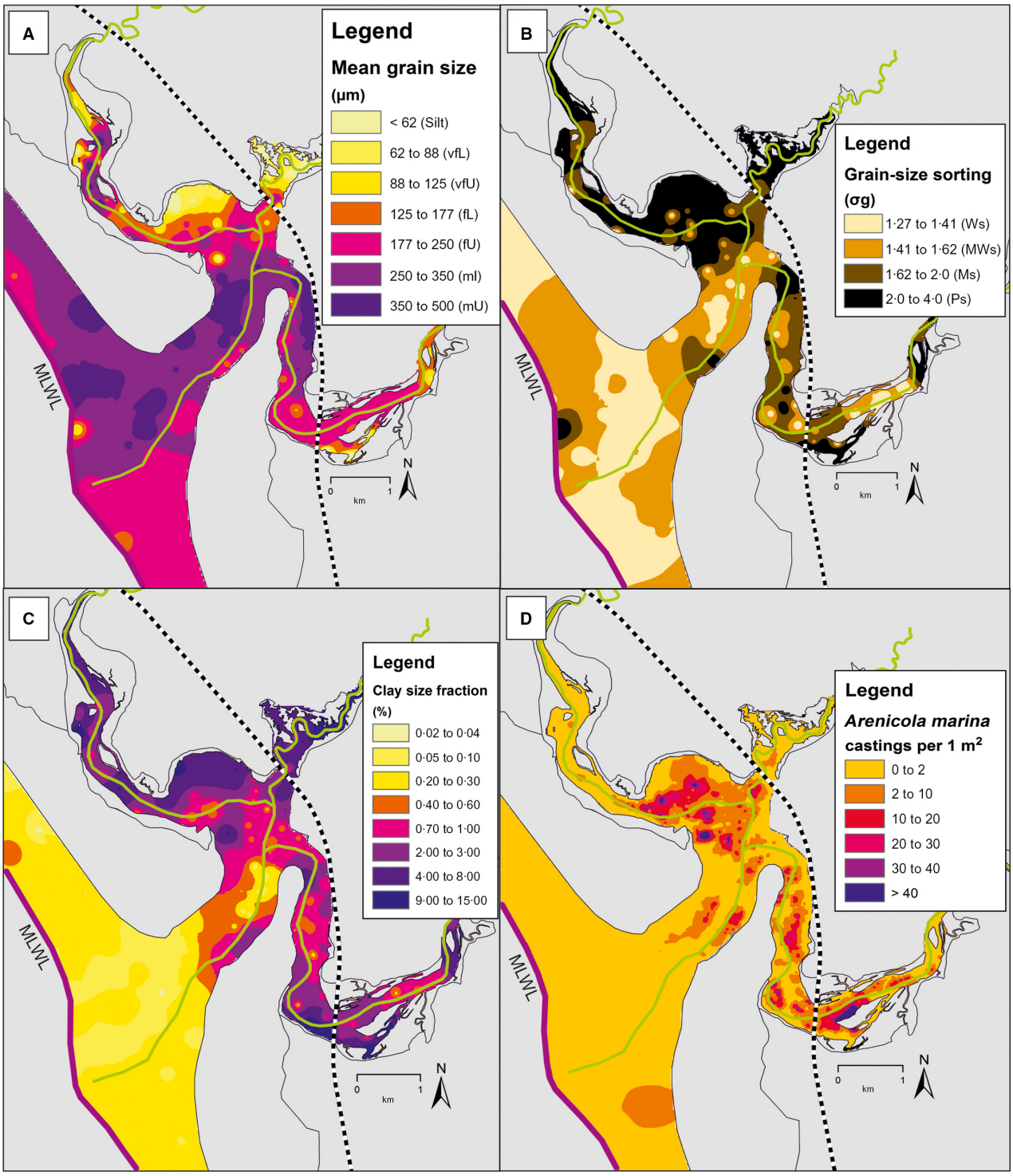

Fig. 8. Distribution of host-sediment properties: (A) mean grain size; (B) grain-size sorting; (C) clay fraction (%); and (D) lugworm (*Arenicola marina*) bioturbation intensity (castings per 1 m^2). MLWL = mean low water line.

are typically finer grained (125 to 250 μm) than deposits upon the northern foreshore and backshore (250 to 500 μm) (Fig. 8A). Sorting ranges from moderately well (1·41 to 1·62 σg) to well-sorted (1·27 to 1·41 σg) within foreshore and backshore deposits (Fig. 8A). The upper-foreshore (here defined as >2 m OD) is typically structureless, whereas wave-formed ripples (typically

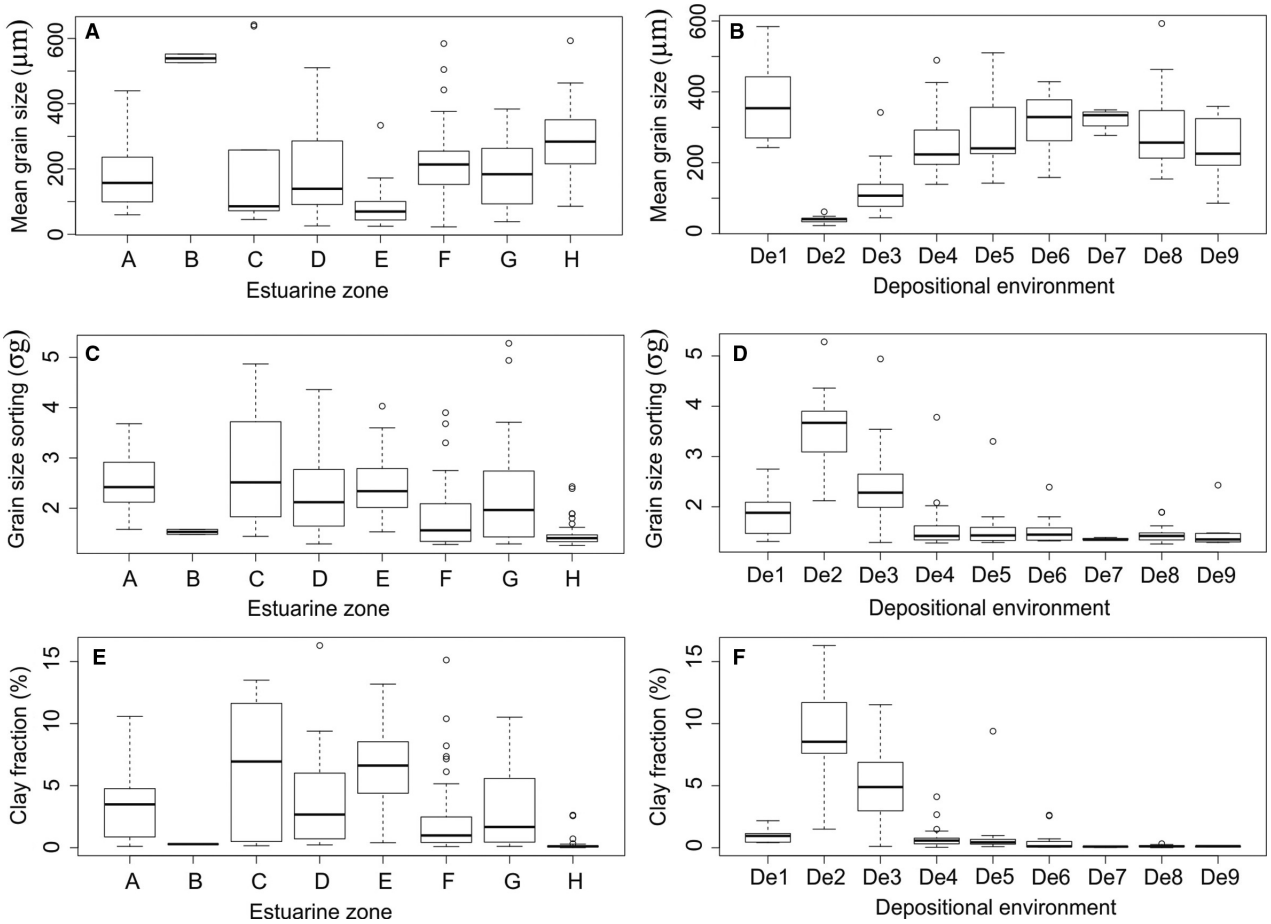

Fig. 9. Mean grain size (A) and (B), grain size sorting (C) and (D) and clay fraction (E) and (F) as a function of estuarine zone (zone A, lower-Irt; zone B lower-Mite; zone C lower-Esk; zone D, inner-Irt; zone E, inner-Mite; zone F, inner, Esk; zone G, central-basin; and zone H, outer-estuary) and depositional environment (De1, gravel-bed; De2, mud-flat; De3, mixed-flat; De4, sand-flat; De5, tidal bars and dunes; De6, tidal-inlet; De7, backshore; De8, foreshore; and De9, pro-ebb delta). Note that outliers (open circles) are defined as an observation that is numerically distant from the rest of the data (i.e. a value that is 1·5 times the interquartile range below the lower quartile and above the upper quartile).

draped by shelly debris) occur upon the lower-foreshore (Fig. 6E; <2 m OD). However, sedimentary structures in the outer estuary are highly dependent upon tidal, wave and wind-conditions that were active during the time of sampling.

Estuarine clay mineral assemblage

On average, across the 171 samples of the main Ravenglass Estuary, the clay mineral assemblage (excluding clays present in sediment >2 μm in size; for example, chlorite-rich lithics) is dominated by illite (average illite index *ca* 0·602), with subordinate quantities of chlorite (average chlorite index *ca* 0·190) and kaolinite (average kaolinite index *ca* 0·208). The estuarine illite is relatively Fe–Mg-rich (average Esquevin Index, 0·315) and well-crystalline (average illite crystallinity index, 0·265) (Table 3).

The average illite, chlorite and kaolinite indices, illite crystallinity and Esquevin Indices have been derived for the nine depositional environments (Table 2; Fig. 7), and for each estuarine zone (Table 3; Fig. 1A) to help understand the relationship between position in the estuary and clay mineralogy. Box and whisker plots display the range and standard deviations as well as the median values for individual depositional environments (Fig. 10) and estuarine zones (Fig. 11). To further understand the relationship between the different types of illite, in terms of crystallinity and chemistry, and position in the estuary, illite crystallinity and Esquevin Index values have been compared by estuary zone (Fig. 12).

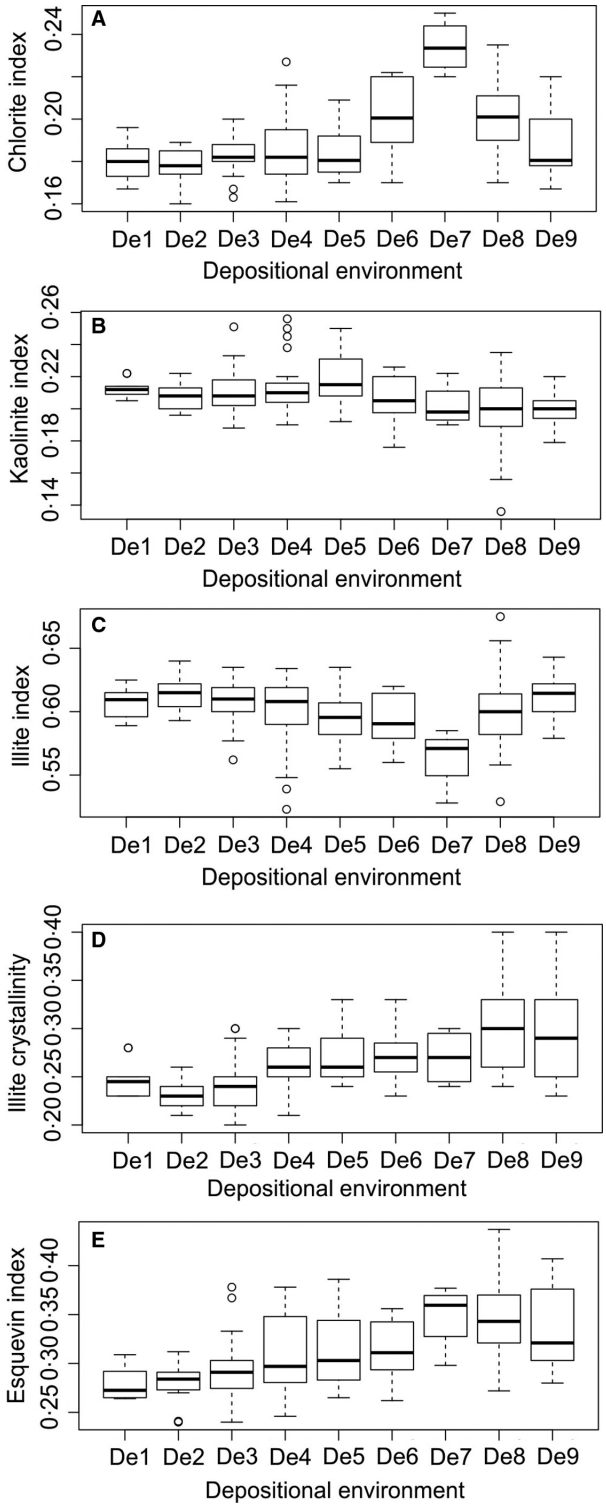

Fig. 10. Relative clay mineral abundance as a function of depositional environment. (A) Chlorite index. (B) Kaolinite index. (C) Illite index. (D) Illite crystallinity (FWHM, full width at half-maximum). (E) Esquevin Index (illite chemistry). Depositional environments, are labelled accordingly: De1, gravel-bed; De2, mud-flat; De3, mixed-flat; De4, sand-flat; De5, tidal bars and dunes; De6, tidal-inlet; De7, backshore; De8, foreshore; and De9, pro-ebb delta. Note that outliers (open circles) are defined as an observation that is numerically distant from the rest of the data (i.e. a value that is 1·5 times the interquartile range below the lower quartile and above the upper quartile).

Mapped estuarine clay mineral distribution

The relative proportions of the three clay minerals, illite, chlorite and kaolinite, have been mapped out using ArcGIS to visualise their distribution patterns.

Chlorite relative abundance is heterogeneous and displays distinct patterns in the Ravenglass Estuary (Fig. 13). Chlorite abundance increases progressively towards the open sea and is highest in backshore and northern foreshore sediments (Fig. 13). In the inner Esk zone, there are subtle increases in relative chlorite abundance with proximity to the ebb-channel, and in tidal-dunes and tidal-bars (Fig. 13). The main ebb-channel, which splits the northern and southern foreshore deposits, is also defined by relative chlorite abundance (Fig. 13); there is distinctly more chlorite in the northern than the southern foreshore deposits.

Kaolinite relative abundance is highest in the central and inner estuary, and is depleted within foreshore sediment (Fig. 14). In the inner/central estuary, kaolinite relative abundance appears to be somewhat random (i.e. lacking organisation) (Fig. 14).

Illite relative abundance is heterogeneous and displays distinct patterns in the Ravenglass Estuary (Fig. 15). Relative illite abundance is highest at the margins of the inner and central estuary and in outer estuarine sediment positioned within/proximal to the ebb-channel (Fig. 15). Illite relative abundance is lowest in the tidal inlet, northern foreshore/backshore, and within tidal bars and tidal dunes (Fig. 15).

Illite composition (derived from the Equevin Index) is heterogeneous and displays distinct patterns in the Ravenglass Estuary (Fig. 16). Mapped Esquevin Indices show that illite is relatively Al-rich (Fe–Mg depleted) towards the open sea. Relatively Fe–Mg-enriched illite is located in the inner and central estuary towards the estuarine margin (Fig. 16). Illite crystallinity is heterogeneous and displays distinct patterns in the Ravenglass Estuary (Fig. 17). Illite is most crystalline (lowest illite crystallinity) in the inner and central estuary, towards the estuarine

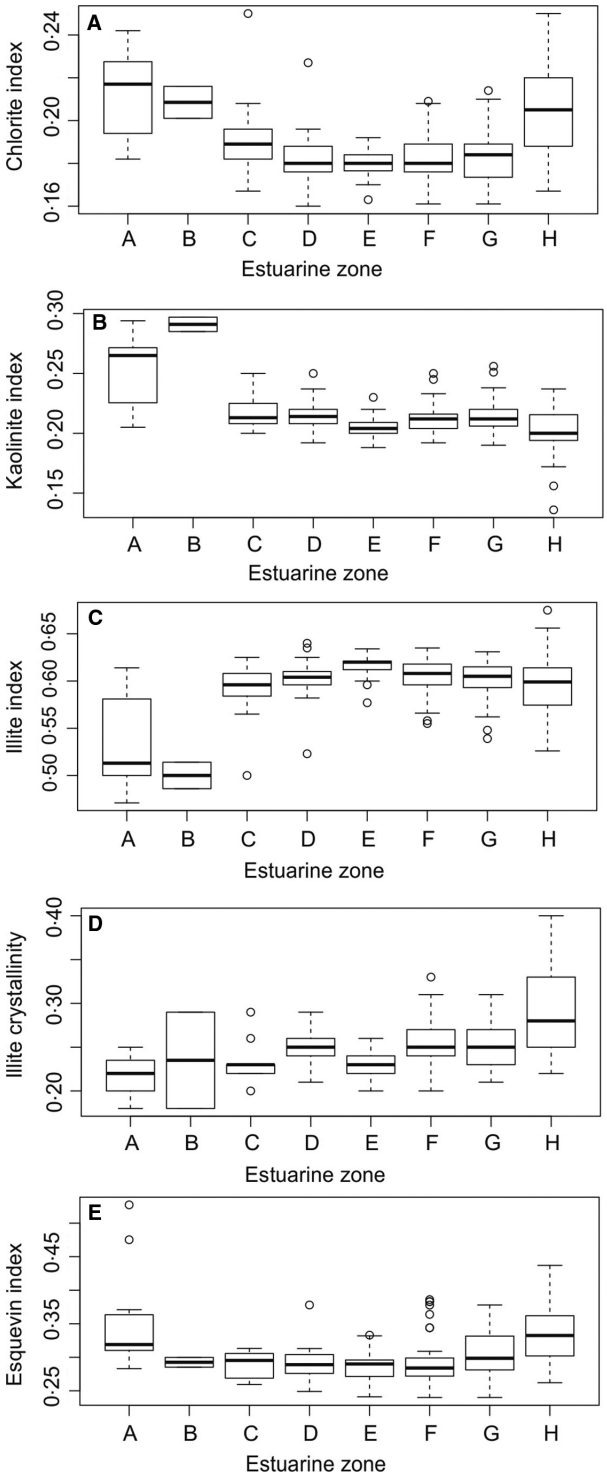

Fig. 11. Clay mineral abundance as a function of estuarine zone. (A) Chlorite index. (B) Kaolinite index. (C) Illite index. (D) illite crystallinity (FWHM, full width at half-maximum). (E) Esquevin Index (illite chemistry). Estuarine zones are labelled accordingly: A, lower-Irt; B lower-Mite; C lower-Esk; D, inner-Irt; E, inner-Mite; F, inner, Esk; G, central-basin; and H, outer-estuary. Estuarine zones are shown in map form on Fig. 1A. Note that outliers (open circles) are defined as an observation that is numerically distant from the rest of the data (i.e. a value that is 1·5 times the interquartile range below the lower quartile and above the upper quartile).

margins (Fig. 17). Illite crystallinity typically decreases (increased FWHM) towards the open-sea (Fig. 17). In the inner estuary, tidal bars and tidal dunes can be differentiated based upon a decrease in both illite crystallinity and Fe–Mg content (Figs 16 and 17).

Clay mineral abundance as a function of grain-size fraction

A central estuary bulk sediment sample, from the Saltcoats mixed-flat, was split into different grain-size fractions in order to determine whether different clay minerals preferentially fall within different grades of sediment. Each size separate was analysed by X-ray diffraction. The relative clay mineral proportions have been plotted versus grain size showing that kaolinite and illite abundances increase as grain size decreases, whereas chlorite abundance increases with increasing grain size (Fig. 18).

Mineralogy of bedrock, drift and upper fluvial deposits

The lithology of the Triassic Sherwood Sandstone, the Palaeozoic Borrowdale Volcanic Group and the Palaeozoic Eskdale Granite has been summarised based on previously published studies (Simpson, 1934; Moseley, 1978; Young *et al.*, 1986; Strong *et al.*, 1994; Merritt & Auton, 2000; Stone & Merriman, 2004; Quirke *et al.*, 2015) (Table 1). The mineralogy of samples of hinterland bedrocks and drift-deposits was determined using XRD to help understand the clay mineralogy of the sediment that is being fed into the estuary. The clay mineralogy and relative quantities of chlorite, kaolinite and illite were determined using the methods described previously. The Esquevin Index of illite could be determined for bedrock samples, but the illite crystallinity could not be determined due to the influence of crystal size of the white mica in rock which has a major influence on the FWHM measurement (Krumm & Buggisch, 1991). The clay mineralogy of the bedrock and drift deposits is listed in Table 4. The mineralogy of upper fluvial sediments was

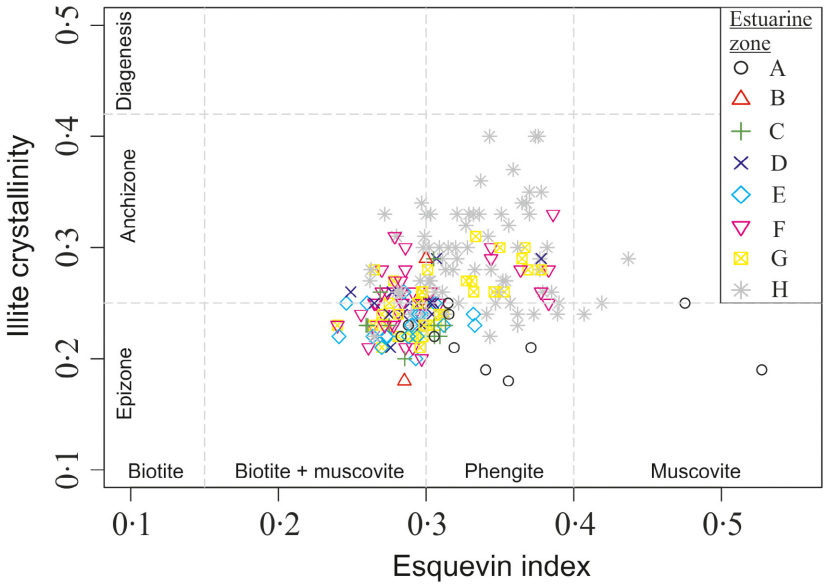

Fig. 12. Variation in Esquevin Index (illite chemistry) and illite crystallinity (FWHM, full width at half-maximum) as a function of estuarine zone. Estuarine zones are labelled accordingly; A, lower-Irt; B lower-Mite; C lower-Esk; D, inner-Irt; E, inner-Mite; F, inner, Esk; G, central-basin; and H, outer-estuary. Estuarine zones are shown in map form on Fig. 1A.

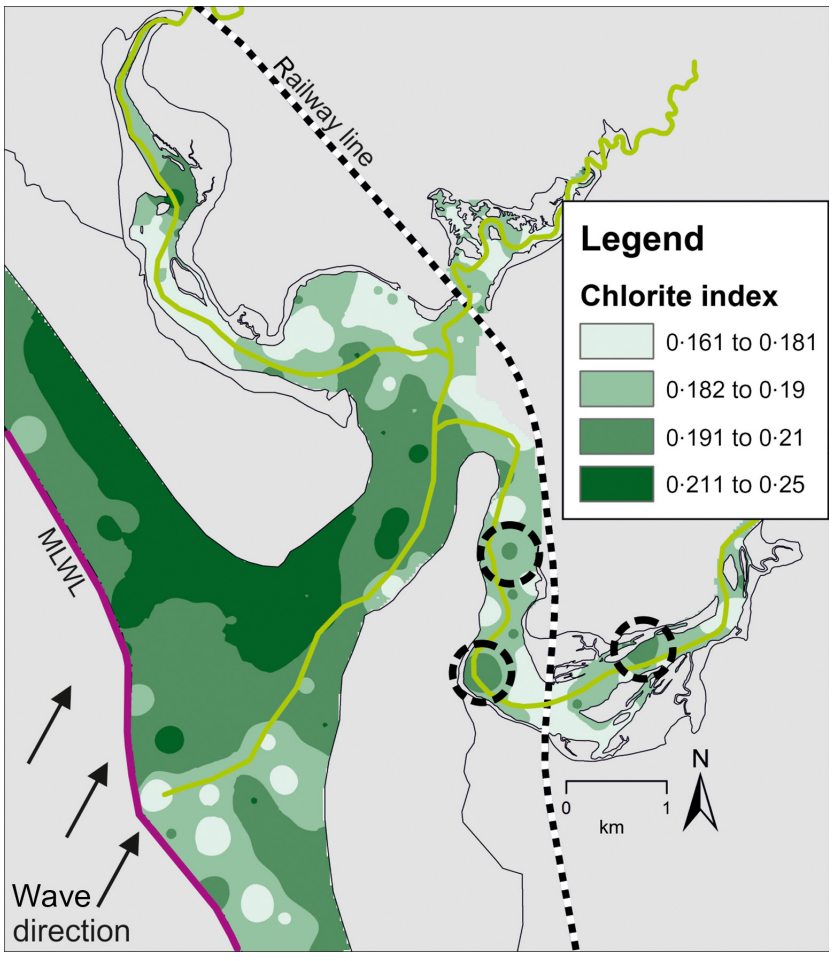

Fig. 13. Chlorite distribution within the Ravenglass Estuary. Black dashed circles highlight relatively chlorite enriched tidal bars and dunes. Black arrows indicate the dominant wave direction, leading to a relatively chlorite-enriched northern foreshore and backshore. The mean low water line (MLWL) is indicated by a solid purple line. Depositional environments are shown in map form on Fig. 7.

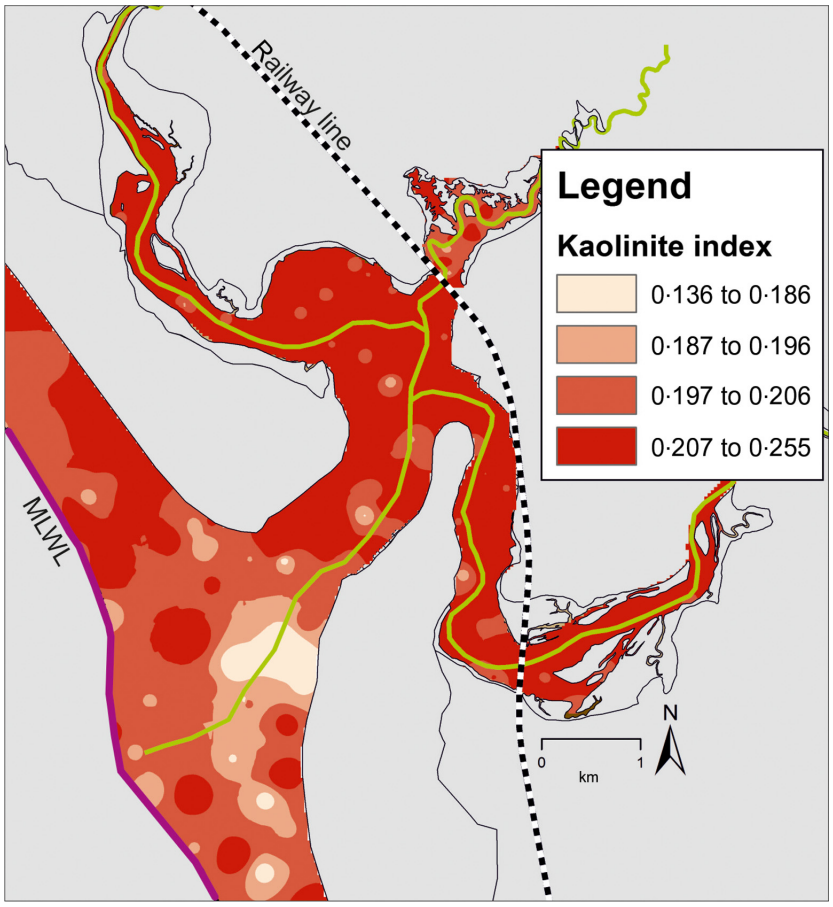

Fig. 14. Kaolinite distribution within the Ravenglass Estuary. Kaolinite abundance is relatively homogenous in the inner estuary and central basin, and relatively depleted in foreshore and pro-ebb delta sediment. The mean low water line (MLWL) is indicated by a solid purple line. Depositional environments are shown in map form on Fig. 7.

also determined by XRD analysis to help understand the sediment supply budget. The relative abundances of chlorite, kaolinite and illite from four fluvial channel samples (Fig. 1) are listed in Table 4.

Statistical analysis of estuarine clay mineral distribution

Pearson's correlation coefficients have been calculated in order to determine whether there are any statistically significant relationships between the characteristics of estuary zones (for example, grain size and sorting) and clay mineralogy for both individual estuarine zones and for the entire mapped estuary (Table 5). Analysis Of Variance (ANOVA) test results show that there is a statistically significant difference ($P < 0{\cdot}05$) in relative clay mineral abundance (chlorite, illite and kaolinite), as well as Esquevin Index and illite crystallinity as a function of both estuarine zone and depositional environment. The multi-comparison, post-hoc Tukey HSD test results show between which estuarine zones (Table 6) and depositional environments (Table 7) there are statistical differences ($P < 0{\cdot}05$) in relative clay mineral abundances, Esquevin Index and illite crystallinity values; marginally significant (†, $P < 0{\cdot}1$) values are also noted.

Summary of estuarine distribution patterns of clay minerals

For the first time, detailed maps of the distribution of clay minerals of an entire estuary have been produced (Figs 13 to 17). To the authors' knowledge, similar high sample-density maps of clay mineral proportions have not been produced for any marine or non-marine modern sedimentary environment. An important output from this work is the observation that clay minerals within the Ravenglass Estuary are not distributed uniformly (Figs 13 to 17).

Chlorite is typically most enriched in the coarsest grain fractions of the estuarine sediment (Fig. 13), whereas illite (Fig. 15) is most abundant in the finest grained fraction. These patterns are confirmed by Pearson's correlation coefficients (Table 5) and X-ray diffraction analysis on grain-size separates (Fig. 18).

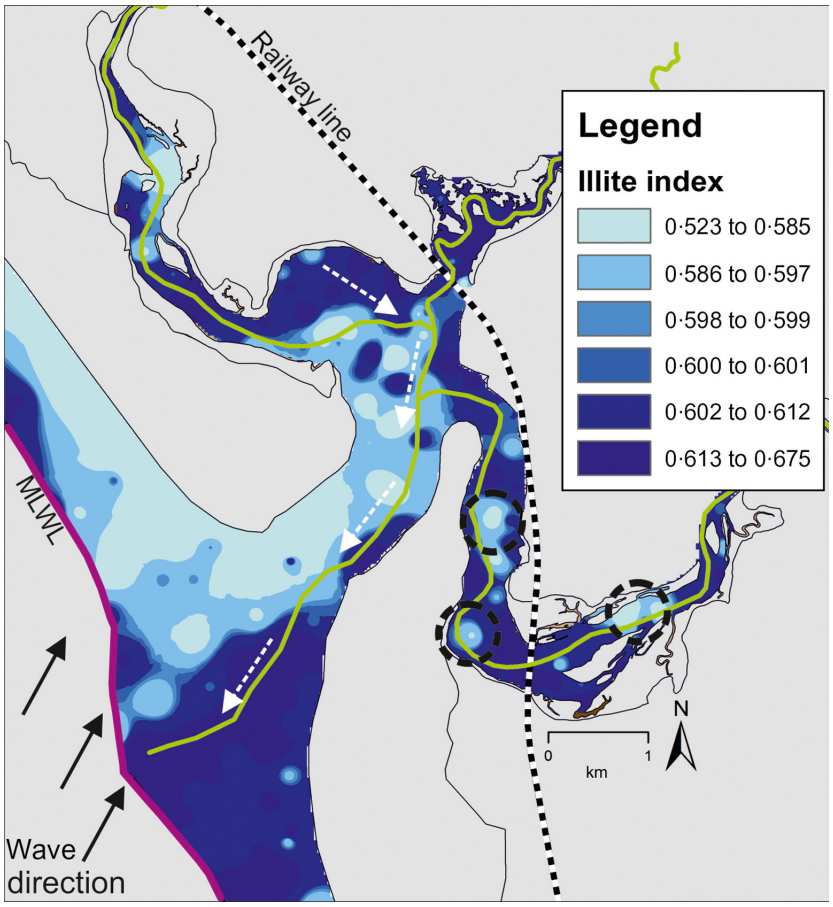

Fig. 15. Illite distribution within the Ravenglass Estuary. Black dashed circles highlight relatively illite depleted tidal bars and dunes. Black arrows indicate the dominant wave direction, leading to a relatively illite depleted northern foreshore and backshore. Dashed white arrows highlight the potential importance of connectivity between the illite enriched central basin and illite enriched southern foreshore. The mean low water line (MLWL) is indicated by a solid purple line. Depositional environments are shown in map form on Fig. 7.

By comparing the clay mineral maps (Figs 13 to 17) with host sediment properties (Figs 7 to 9) for the inner and central parts of the estuary, and reference to Tables 5 and 6, it can be concluded that illite is most abundant towards the estuarine margins (mixed and mud-flats). In contrast, relatively high-energy, coarse-grained and well-sorted, inner and central zone facies, i.e. tidal bars and dunes and channel axis, are relatively illite-depleted and relatively enriched in chlorite and kaolinite (Figs 13 and 14; Tables 5 and 6). As well as localisation of illite, kaolinite and chlorite as a function of position in the estuary, the types of illite (composition and crystallinity) reveal spatial patterns. The illite at the estuarine margins is predominantly well crystalline (low FWHM value) and Fe–Mg-rich (low Esquevin Index value). The illite in the relatively high-energy, coarse-grained, and well-sorted, inner and central zone facies is relatively enriched in structurally and chemical degraded forms of illite with high FWHM values and high Esquevin Index values (Figs 15 to 17).

Outer estuarine sediment is relatively depleted in kaolinite (Fig. 14; Table 6). Outer estuarine sediment (backshore and upper foreshore) is relatively enriched in chlorite, north of the main channel outlet (Fig. 13). In contrast, illite is most abundant in the outer estuary in the ebb channel outlet, and the area to the south of the ebb-channel (Fig. 15). Outer estuarine sediment contains illite that is relatively poorly-crystalline (high FWHM values) and Al-rich (high Esquevin Index values) (Figs 16 and 17). However, there is a plume of relatively Fe–Mg-rich illite (low Esquevin Index values) that is associated with the mouth of the estuary (Fig. 16).

DISCUSSION: CONTROLS ON ESTUARINE CLAY MINERAL DISTRIBUTION

Clay minerals are not homogenously distributed in the Ravenglass Estuary (Figs 13 to 17). In order to develop models that can be employed in schemes to help facilitate reservoir quality

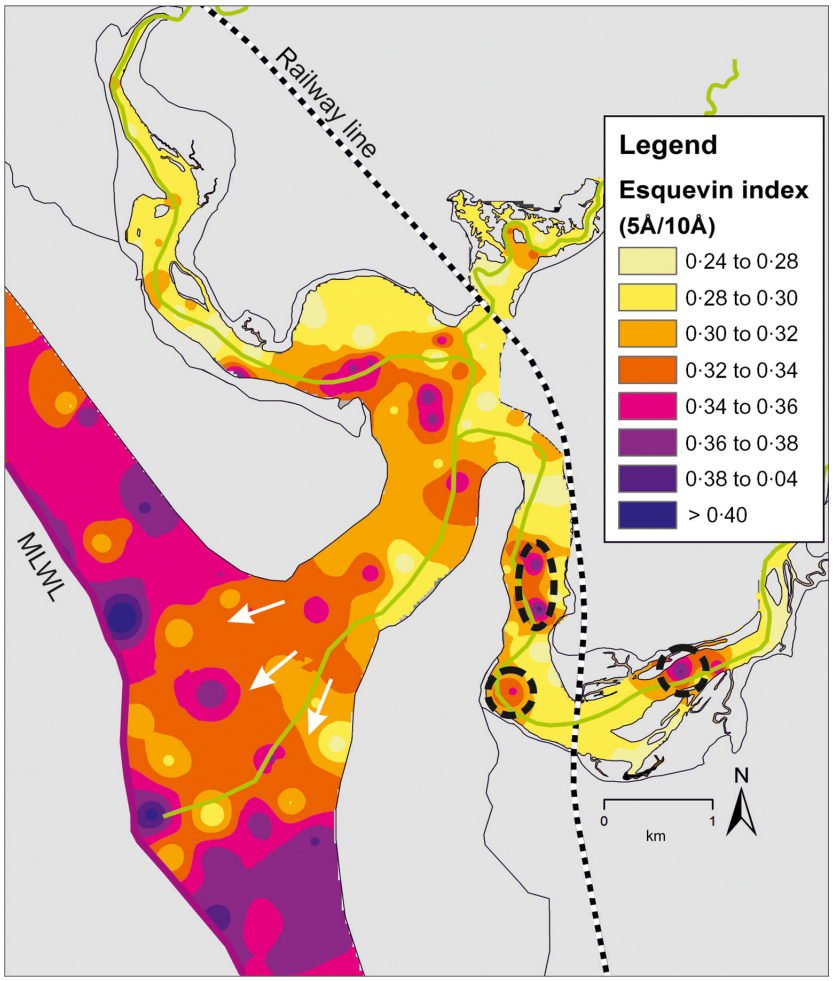

Fig. 16. Esquevin Index distribution within the Ravenglass Estuary. Black dashed circles highlight tidal bars and dunes enriched in poorly crystalline illite. White arrows depict the plume of relatively Fe–Mg enriched illite (inner and central estuarine derived) mixing with the relatively Al-enriched illite upon the foreshore. The mean low water line (MLWL) is indicated by a solid purple line. Depositional environments are shown in map form on Fig. 7.

prediction in ancient, deeply buried marginal marine sandstones, it is imperative to determine what has controlled the distribution of clay minerals in the Ravenglass Estuary.

Potential sources of clay minerals in the Ravenglass estuary

In order to explain the clay mineralogy of the estuary, it is necessary to consider the clay mineralogy of all potential sources. The suite of clay minerals fed into the Ravenglass Estuary may be derived from a combination of: (i) fluvial drainage of bedrock (Fig. 1A; Tables 1 and 4); (ii) fluvial drainage of Quaternary drift deposits, including local erosion of Ravenglass Till within the margins of the estuary (Fig. 1B; Table 1); and (iii) marine inundation, with the landward displacement of littoral-zone sediment.

The clay mineralogy of the upper fluvial inputs (Table 4) is distinctly different to the average clay mineralogy of the estuary, as shown by Tables 2 and 3. The sediment delivered by the River Irt has relatively high kaolinite and chlorite indices and a commensurately low illite index (Table 4). Illite in the River Irt has high Esquevin Indices representing Fe–Mg-poor mica (Table 4). The sediment delivered by the River Esk is even more dominated by chlorite than the River Irt and has a low illite index (Table 4). Like the River Irt, illite in the River Esk also has a high Esquevin Index (Table 4).

Ravenglass Till underlies and surrounds the Ravenglass Estuary (Table 1). The till is exposed in localised cliff sections to the east of the northern part of the upper Esk Estuary (Fig. 1), just south of Ravenglass village. The glacial till is dominated by illite (illite index, 0·62) and the illite is both relatively Fe–Mg-rich (Esquevin Index, 0·28), and well-crystalline (illite crystallinity, 0·24). The Ravenglass Till has a moderate abundance of kaolinite (kaolinite index, 0·21), and is relatively depleted in chlorite (chlorite index, 0·17).

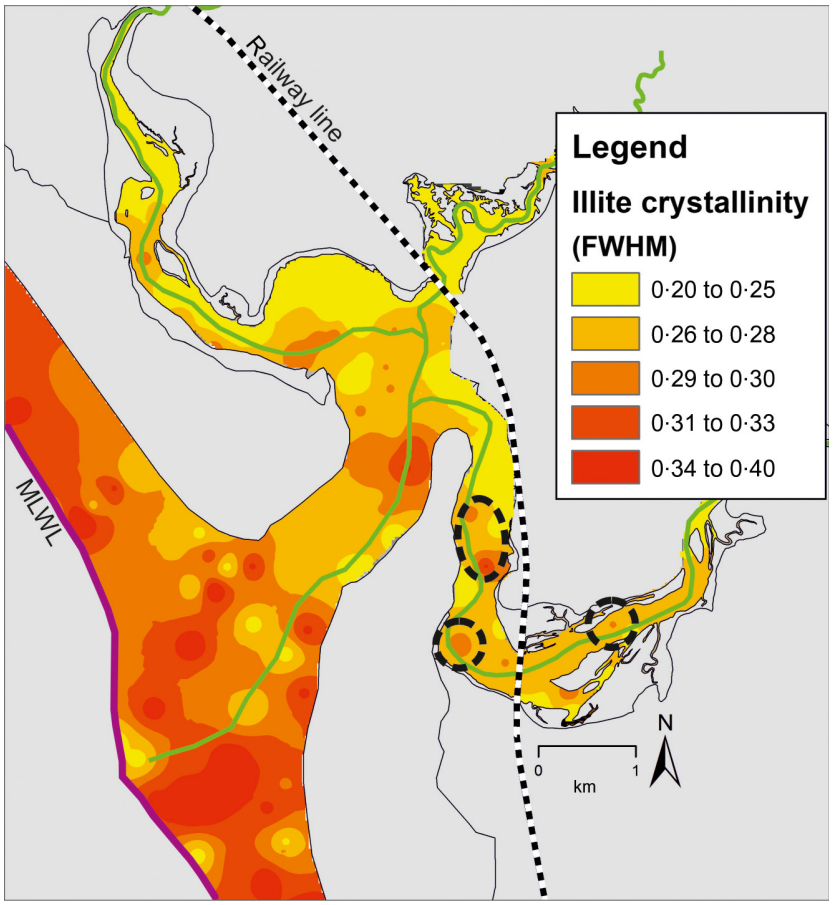

Fig. 17. Illite crystallinity (FWHM, full width at half-maximum) distribution within the Ravenglass Estuary. Black dashed circles highlight tidal bars and dunes enriched in Al-rich illite. The mean low water line (MLWL) is indicated by a solid purple line. Depositional environments are shown in map form on Fig. 7.

Littoral zone grab-samples from below the low water mark could not be collected on the advice of the UK's Ministry of Defence, due to the high risk of unexploded ordnance, because the area has been a testing-ground for large calibre conventional weapons since 1903. However, many samples were collected from the littoral zone between the high and low water marks in zone H (Figs 1 and 3) with their clay mineralogy presented in Tables 2 and 3 and Figs 9 to 17. It will be shown subsequently that the littoral zone receives an amalgamation of sediment from the estuary, which is supplied by the glacial till and fluvial discharge from the hinterland.

As established here (Tables 2 and 3; Figs 10 to 17), the clay mineral distribution in the Ravenglass Estuary is heterogeneous. There are three possible influences on clay mineral type and distribution: supply types (provenance); hydrodynamics (transport and deposition); and early diagenesis (post depositional processes). The sections below discuss which sources and processes together explain the distribution of the clay minerals.

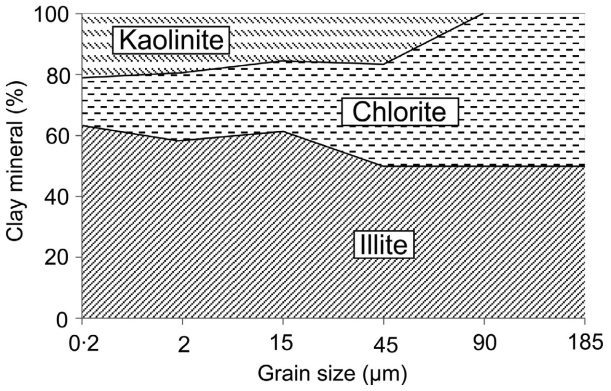

Fig. 18. Relative clay mineral abundance as a function of disaggregated grain-size separates, extracted from a singular central-basin sediment sample.

Provenance control on clay mineral distribution

The estuarine sediment has average illite, chlorite and kaolinite indices of about 0·60, 0·19 and 0·21, respectively. In addition, the estuarine sediment has average Esquevin and illite

Table 4. Chlorite, kaolinite and illite indices and the Esquevin Index and illite crystallinity (FWHM, full width at half-maximum) in upper-fluvial riverine sediment from the Ravenglass area and bedrock and drift clay mineralogy and Esquevin Index data. All data generated within this study except the Esquevin Index data from the Skiddaw Slate that is taken from Stone & Merriman (2004).

	Chlorite index	Kaolinite index	Illite index	Esquevin index (5Å/10Å)	Illite crystallinity (FWHM)
River Irt-1	0·39	0·39	0·22	0·47	0·20
River Irt-2	0·24	0·30	0·45	0·38	0·19
River Esk-1	0·58	0·25	0·17	0·48	0·23
River Esk-2	0·57	0·17	0·27	0·48	0·26
Fishgarth Till	0·08	0·31	0·61	0·43	0·21
Ravenglass Till	0·17	0·21	0·62	0·28	0·24
St Bees sandstone	–	–	–	0·36	–
Eskdale granite-1	–	–	–	0·16	–
Eskdale granite-2	–	–	–	0·35	–
Skiddaw slate	–	–	–	0·4	–

crystallinity indices of 0·31 and 0·26, respectively (Tables 2 and 3; Figs 10 to 17). However, the variability of these values shows that it is possible that there have been different sources of clay minerals fed into different parts of the estuary. An initial, simplistic, view of sediment in the Ravenglass Estuary could be that the sediment was delivered directly from the mountainous English Lake District to the east of the coastline, via the rivers Irt and Esk.

Upper fluvial Esk sediment samples (Fig. 1) are strongly chlorite-enriched and the upper fluvial Irt samples are moderately-enriched in chlorite compared with the estuarine sediment (Tables 2 to 4). The Esk chlorite-enrichment probably reflects the widespread hydrothermal chloritisation of biotite and hornblende in the Eskdale Granite (Table 1) (Moseley, 1978; Young *et al.*, 1986). The Irt chlorite-enrichment probably reflects the widespread hydrothermal chloritisation of biotite and hornblende in the Eskdale Granite, and/or pseudomorphs after pyroxene in the Borrowdale Volcanic Group (Table 1) (Quirke *et al.*, 2015).

The upper and lower fluvial Irt samples (Fig. 1) are significantly enriched in kaolinite (Table 4). By analogy to the Esk sediment, it could be expected that the kaolinite was derived from the hinterland bedrock (Borrowdale Volcanic Group and Sherwood Sandstone; Table 1), although this is not reported to be enriched in kaolinite. Instead, the kaolinite may have been derived from locally kaolinite-enriched, glaciolacustrine sediment of the Gosforth Glaciogenic Formation (Fig. 1; Tables 1 and 4). Provenance has previously been reported to explain the enrichment of kaolinite in the kaolinite-enriched fluvial sediment landward of Chesapeake Bay (Hathaway, 1972) due to the drainage of kaolinite-enriched Piedmont (Neiheisel & Weaver, 1967).

The upper fluvial Esk and Irt samples are generally depleted in illite (Table 3) compared to the estuarine deposits (Tables 2 to 4; Fig. 11). In contrast to the sediment in the estuary (Tables 2 and 3), the illite present in the upper fluvial Esk and Irt samples are relatively Al-rich with much higher Esquevin Indices (mostly greater than 0·40) than the estuarine sediment (Table 4). This probably reflects the relatively advanced stage of weathering of micas in the hinterland (Eskdale Granite, Sherwood Sandstone and Borrowdale Volcanic Group; Table 1) in contrast to the supply of micas into the estuary. A key point is that the estuarine sediment (Table 3) does not closely compare to the supply of sediment being delivered by the rivers (Tables 2 to 4; Figs 9 to 12).

The presence of eroding low cliffs of the Quaternary Ravenglass Till that surround part of the estuary strongly suggests that some of the sediment in the estuary may be supplied by this till. The gravel beds exposed at the surface in the lower Esk estuary appear to be directly formed from the erosion of nearby pebble and cobble bearing Ravenglass Till. Glacial till is also exposed as knolls in all zones within the estuary. The relatively well-crystalline and Fe-Mg-rich illite in the Ravenglass Estuary is typical of glacial deposits (such as the Ravenglass Till), which are formed under cold-climatic conditions that result in mechanical weathering allowing the mica (illite) to retain its original high degree of crystallinity and Fe–Mg-rich composition

Table 5. Pearson's correlation coefficient results for individual estuarine zones showing the strength of the relationship between relative clay mineral abundance (chlorite, illite and kaolinite), Esquevin Index and illite crystallinity (FWHM), in relation to mean grain size (MGS), grain size sorting (GSS), clay fraction abundance (CF), sand percentage (S), bioturbation intensity (Biot.) and elevation (Elev.).

	MGS	GSS	CF	S	Biot.	Elev.
River Irt (A), n = 11						
Chlorite	**0·60***	−0·41	−0·48	0·34	na.	na.
Illite	−0·48	0·28	0·49	−0·39	na.	na.
Kaolinite	0·37	−0·48	−0·48	0·29	na.	na.
FWHM	0·09	−0·08	−0·06	0·06	na.	na.
Esq. I	**0·78****	−0·48	**−0·53**†	0·50	na.	na.
Inner Irt (D), n = 19						
Chlorite	0·30	−0·22	**−0·44**†	0·22	−0·14	−0·37
Illite	**−0·56****	**0·40**†	**0·59****	**−0·46***	0·19	0·31
Kaolinite	**0·71*****	**−0·48***	**−0·61****	**0·60****	−0·21	−0·25
FWHM	0·36	−0·04	−0·12	0·20	0·01	−0·02
Esq. I	0·32	**−0·52***	−0·29	0·35	−0·25	−0·02
Inner Esk (F), n = 37						
Chlorite	0·13	−0·12	−0·11	0·15	−0·22	−0·59
Illite	−0·26	0·27	**−0·43****	−0·22	**0·37***	0·26
Kaolinite	**0·29**†	**−0·31**†	**−0·42****	0·22	**−0·38***	−0·26
FWHM	0·17	**−0·50****	**−0·39***	0·17	−0·27	−0·02
Esq. I	0·23	**−0·42***	**−0·49****	**0·35***	−0·10	−0·23
Outer estuary (H), n = 75						
Chlorite	**0·67*****	**−0·30***	**−0·28***	0·08	**−0·29***	**0·49*****
Illite	**−0·56*****	0·11	0·16	−0·05	0·12	**−0·46*****
Kaolinite	0·15	0·15	0·06	0·00	0·12	0·17
FWHM	**−0·22**†	−0·09	0·04	0·04	−0·17	−0·11
Esq. I	0·12	−0·21	−0·16	0·00	−0·05	**−0·22**†
River Esk (C), n = 10						
Chlorite	**0·76****	−0·31	−0·51	**0·58**†	na.	na.
Illite	**−0·63***	0·1	0·35	**−0·56**†	na.	na.
Kaolinite	0·31	0·23	−0·07	0·44	na.	na.
FWHM	0·50	**−0·66***	−0·23	0·41	na.	na.
Esq. I	−0·12	0·36	0·32	−0·04	na.	na.
Inner Mite (E), n = 19						
Chlorite	0·04	−0·20	−0·24	0·35	0·36	0·13
Illite	0·07	0·11	0·20	−0·24	−0·34	−0·13
Kaolinite	−0·15	−0·01	−0·10	0·06	0·21	0·08
FWHM	0·11	0·03	−0·32	0·31	0·13	−0·17
Esq. I	−0·04	0·07	0·09	−0·06	0·08	0·30

Table 5. (continued)

	MGS	GSS	CF	S	Biot.	Elev.
Central basin (G), $n = 35$						
Chlorite	**0·32**†	−0·16	−0·17	−0·12	−0·11	−0·11
Illite	−0·14	0·06	0·25	0·29	0·25	**0·36**†
Kaolinite	−0·05	0·05	−0·24	**−0·35**†	−0·28	**−0·45***
FWHM	**0·55****	**0·44****	**−0·59*****	**0·33**†	0·11	**−0·47***
Esq. I	0·28	−0·20	**−0·48****	0·02	0·25	**−0·44***
Inner, central, outer, $n = 185$						
Chlorite	**0·52*****	**−0·35*****	**−0·39*****	**−0·16**†	**−0·14**†	0·07
Illite	**−0·43*****	**0·20***	**0·32*****	0·12	**0·14**†	−0·11
Kaolinite	0·04	0·11	−0·02	−0·11	−0·05	**0·13**†
FWHM	**0·30*****	**−0·42*****	**−0·47*****	**0·35*****	−0·07	**−0·32*****
Esq. I	**0·20*****	**−0·40*****	**−0·45*****	**0·30*****	0·03	**−0·36*****

Levels of statistical significance are coded as follows; marginally significant †when $P < 0{\cdot}1$, significant *when $P < 0{\cdot}05$, very significant **when $P < 0{\cdot}01$, extremely significant ***when $P < 0{\cdot}001$. Values without bold represent no significant difference when $P > 0{\cdot}1$. Estuarine zones are shown in map form on Fig. 1A. FWHM, full width at half-maximum.

(Chamley, 1989). There is a similarity between the illite-dominated clay mineral assemblage, illite chemistry and illite crystallinity of the Ravenglass Till and the Ravenglass Estuary sediment (Tables 1 to 4; Figs 9 to 12). However, it is likely that there are multiple sources of illite in the drainage basin (Table 1) and in the Ravenglass Estuary, given the range in Esquevin Indices (Fig. 12) and the range of chlorite enrichments found within the estuary (Fig. 13). It thus seems likely that any fluvial supply of sediment, with high Esquevin Indices and relatively enriched in chlorite (Table 4), is being heavily diluted by a second sediment source with a distinct clay mineral suite, such as from the eroding Ravenglass Till exposed within, and at the margins of, the Ravenglass Estuary.

Hydrodynamic control on clay mineral distribution

As well as there being several possible sources of the clay minerals in the Ravenglass Estuary, it is also possible that estuarine hydrodynamics has influenced the distribution of clay minerals. The pair of barrier spits have resulted in the Ravenglass Estuary having wave-dominated morphological characteristics (Dalrymple *et al.*, 1992). Such estuaries typically have high energy outer regions, inner regions that are wave and river-dominated, and a low energy central basin. It is likely that typical wave-dominated estuaries will have coarse-grained outer and inner regions separated by a fine-grained central region (Dalrymple *et al.*, 1992). The Ravenglass Estuary, however, does not display a well-defined tripartite zonation (outer, central and inner) in grain size (Figs 8A and 9A) or clay fraction (Figs 8C and 9E). It is likely that a combination of the following factors have led to the boundaries between the central and inner estuarine zones of the Ravenglass Estuary being blurred: (i) strong tidal currents pass beyond the low-energy, central basin into the inner parts of the estuary producing extensive tidal bars and tidal dune complexes; and (ii) the Ravenglass Estuary is in the later stages of filling (as shown by the presence of the pro-ebb delta) which has been reported to reduce the significance of the energy-minimum in the central part of an estuary (Posamentier & Walker, 2006). Additionally, forced regression, with a gradual relative sea-level fall following a minor highstand (1 m above Ordnance Datum) at *ca* 6000 years BP (mid-Holocene) (Lloyd *et al.*, 2013), is reported to have caused the coarsening-

Table 6. Matrix comparing clay mineralogy data between the various estuarine zones from the Ravenglass Estuary.

	A	B	C	D	E	F	G
Chlorite Index							
B	−0·00	X					
C	−0·01	−0·02	X				
D	**−0·03*****	−0·03	−0·01	X			
E	**−0·03*****	−0·03	−0·01	−0·00	X		
F	**−0·03*****	−0·03	−0·01	−0·00	0·00	X	
G	**−0·03*****	−0·02	−0·01	0·00	0·00	0·00	X
H	−0·03	−0·01	0·01	**0·02*****	**0·02*****	**0·02*****	**0·20*****
Illite Index							
B	−0·04	X					
C	**0·05*****	**0·09*****	X				
D	**0·07*****	**0·10*****	0·01	X			
E	**0·08*****	**0·12*****	0·03	0·01	X		
F	**0·08*****	**0·15*****	0·02	0·00	−0·01	X	
G	**0·06*****	**0·10*****	0·013	−0·00	−0·01	−0·00	X
H	**0·06*****	**0·09*****	0·01	−0·01	**−0·02**†	−0·01	−0·01
Esquevin index (5Å/10Å)							
B	0·02	X					
C	0·02	0·00	X				
D	0·03	0·01	0·02	X			
E	0·01	0·00	0·00	0·00	X		
F	**0·04*****	0·02	0·02	0·01	0·02	X	
G	**0·03*****	0·02	0·02	0·00	0·02	0·00	X
H	**0·07*****	0·05	**0·06*****	**0·04*****	**0·06*****	**0·03*****	**0·04*****
Kaolinite Index							
B	**0·04***	X					
C	**−0·03*****	**−0·07*****	X				
D	**−0·04*****	**−0·08*****	0·00	X			
E	**−0·05*****	**−0·09*****	−0·01	−0·01	X		
F	**−0·04*****	**−0·08*****	−0·01	0·00	0·01	X	
G	**−0·04*****	**−0·08*****	0·00	0·00	0·01	0·00	X
H	**−0·05*****	**−0·09*****	**−0·02**†	**−0·01***	0·00	**−0·01***	**−0·01***

Table 6. (continued)

	A	B	C	D	E	F	G
Illite crystallinity (FWHM)							
B	0·02	X					
C	0·02	0·00	X				
D	0·03	0·01	0·02	X			
E	0·01	−0·01	0·00	−0·02	X		
F	**0·04***	0·02	0·02	0·01	0·02	X	
G	**0·03**†	0·02	0·02	0·00	0·02	0·00	X
H	**0·07*****	0·05	**0·06*****	**0·04*****	**0·06*****	**0·03*****	**0·04*****

Post-hoc Tukey's honestly significant difference (HSD) test to determine whether there is a statistically significant variation in clay mineral abundance, Esquevin Index and illite crystallinity between individual estuarine-zones. The estuarine zones are labelled accordingly: A, lower-Irt; B, lower-Mite; C, lower-Esk; D, inner-Irt; E, inner-Mite; F, inner, Esk; G, central-basin; and H, outer-estuary. Levels of statistical significance are coded as follows; marginally significant †when $P < 0{\cdot}1$, significant *when $P < 0{\cdot}05$, very significant **when $P < 0{\cdot}01$, extremely significant ***when $P < 0{\cdot}001$. Values without bold represent no significant difference when $P > 0{\cdot}1$. Estuarine zones are shown in map form on Fig. 1A. FWHM, full width at half-maximum.

upward of central basin tidal flats (Daneshvar & Worden, 2018), further blurring the differences between the estuarine zones.

Within individual estuarine zones, the relative abundance of chlorite, the dominant illite type (Al-rich versus Fe–Mg-rich), and dominant illite crystallinity (low to high illite crystallinity) appear to be controlled by estuarine-hydrodynamics. In the lower-energy parts, at the margins of the inner estuary and central basin, the finest deposits are dominated by the mineral characteristics of the Ravenglass Till (illite-dominated, and relatively Fe–Mg-rich and well-crystalline illite that has low Esquevin and FWHM indices). In contrast, in the higher energy sites, i.e. tidal bars and dunes and channel axis, the coarsest inner and central zone sediment, are relatively enriched in chlorite and illite that were derived from the fluvial supply of sediment from the hinterland (chemically-degraded forms of illite with high Esquevin Indices). Within higher-energy, outer estuarine sediment, relative chlorite abundance increases with an increase in grain size ($r = 0{\cdot}67$) and elevation ($r = 0{\cdot}49$); this is interpreted to reflect the dominant wave-direction originating from the south-west (Fig. 13; Table 5). Note that chlorite is most abundant in the coarsest grained sediment fractions (Fig. 18), explaining the strong grain-size control on chlorite abundance, at least in the outer estuary zone. Also in the outer estuary, illite is most abundant towards the ebb-channel (Fig. 15); this is interpreted to reflect the hydrodynamic connectivity between the southern foreshore, and the illite-enriched central basin. Evidence for this connection comes from: (i) a distinct increase in relative illite abundance upon the southern-foreshore, at the mouth of the ebb-channel (Fig. 15); and (ii) an enrichment of relatively Fe–Mg-rich (low Esquevin Index) illite at the mouth of the tidal-inlet, interpreted to be sourced from the Fe–Mg-rich illite-dominated inner and central estuarine zones (Fig. 17).

Kaolinite is abundant in fluvial sediments (Fig. 11; Table 4) and probably reflects the drainage of kaolinite-enriched source sediment (specifically the Gosforth Glaciogenic Formation). However, the controls on the distribution of kaolinite at the fluvial–marine interface, and within estuarine sediments of the Ravenglass Estuary are less clear. Three mechanisms have been invoked to explain the distribution of kaolinite in marginal-marine systems: (i) kaolinite flocculates at low salinity (Whitehouse *et al.*,

Table 7. Matrix comparing clay mineralogy data between the various depositional environments from the Ravenglass Estuary.

	De1	De2	De3	De4	De5	De6	De7	De8
Chlorite index								
De2	0·01	X						
De3	0·00	0·01	X					
De4	0·01	0·01	0·00	X				
De5	0·00	0·01	0·00	0·00	X			
De6	**0·02****	**0·02****	**0·02****	**0·01**†	**0·02**†	X		
De7	**0·05*****	**0·06*****	**0·05*****	**0·05*****	**0·05*****	**0·03****	X	
De8	**0·02*****	**0·02*****	**0·02*****	**0·02****	**0·02****	0·00	**−0·03*****	X
De9	0·00	0·01	0·00	0·00	0·00	−0·01	**−0·04*****	−0·01
Kaolinite index								
De2	−0·01	X						
De3	0·00	0·00	X					
De4	0·00	0·01	0·00	X				
De5	0·01	0·01	0·01	0·01	X			
De6	−0·01	0·00	0·00	−0·01	−0·01	X		
De7	−0·01	−0·01	−0·01	−0·01	−0·01	0·00	X	
De8	−0·01	−0·01	**−0·01***	**−0·02****	**−0·02*****	−0·01	0·00	X
De9	−0·01	−0·01	−0·01	−0·01	**−0·02**†	−0·01	0·00	0·00
Illite index								
De2	0·01	X						
De3	0·00	−0·01	X					
De4	−0·01	−0·01	−0·02	X				
De5	−0·01	−0·02	−0·01	0·00	X			
De6	−0·01	−0·02	−0·01	−0·01	0·00	X		
De7	**−0·04***	**−0·05****	**−0·04****	**−0·04**†	−0·03	−0·03	X	
De8	−0·01	−0·02	−0·01	0·00	0·00	0·01	**0·04**†	X
De9	−0·01	−0·02	0·01	0·01	0·02	0·02	**0·05****	0·01
Illite crystallinity (FWHM)								
De2	−0·02	X						
De3	−0·01	0·01	X					
De4	0·01	0·03	0·02	X				
De5	0·02	**0·04**†	**0·03***	0·01	X			
De6	0·02	**0·04**†	**0·03**†	0·01	0·00	X		
De7	0·02	0·04	0·03	0·01	−0·00	−0·00	X	
De8	**0·05*****	**0·07*****	**0·06*****	**0·04*****	**0·03**†	0·03	0·03	X
De9	**0·047***	**0·06*****	**0·06*****	0·03	0·02	0·02	0·02	−0·01

Table 7. (continued)

	De1	De2	De3	De4	De5	De6	De7	De8
Esquevin Index (5Å/10Å)								
De2	0·00	X						
De3	0·01	0·01	X					
De4	0·03	0·03	0·01	X				
De5	**0·04**†	**0·04**†	0·03	0·01	X			
De6	0·04	0·03	0·02	0·01	−0·01	X		
De7	**0·07****	**0·07****	**0·06***	0·04	0·03	0·03	X	
De8	**0·07*****	**0·07*****	**0·05*****	**0·04*****	0·03	0·03	−0·04	X
De9	**0·06*****	**0·06****	**0·04*****	0·03	0·02	0·02	−0·01	−0·01

Post-hoc Tukey's honestly significant difference (HSD) test to determine whether there is a statistically significant variation in clay mineral abundance, Esquevin Index and illite crystallinity between individual depositional environments. The depositional environments are labelled accordingly: De1, gravel-bed; De2, mud-flat; De3, mixed-flat; De4, sand-flat; De5, tidal bars and dunes; De6, tidal-inlet; De7, backshore; De8, foreshore; and De9, pro-ebb delta. Levels of statistical significance are coded as follows; marginally significant †when $P < 0{\cdot}1$, significant *when $P < 0{\cdot}05$, very significant **when $P < 0{\cdot}01$, extremely significant ***when $P < 0{\cdot}001$. Values without bold represent no significant difference when $P > 0{\cdot}1$. FWHM, full width at half-maximum.

1960), thus sediment at the fluvial–marine interface is likely to be relatively enriched in kaolinite; (ii) Edzwald & O'Mella (1975) suggested that illite remains suspended longer than kaolinite (slower aggregation rate), and is thus deposited downstream relative to kaolinite; and (iii) kaolinite-enriched fluvial sediment is diluted by an additional source of less kaolinite-rich sediment within the estuary (Feuillet & Fleischer, 1980).

Although there appears to be a slight increase in the relative concentration of kaolinite in the inner and central estuarine zone, there is no evidence for kaolinite enrichment at the head of the estuary. This suggests that clay mineral distribution cannot be explained by differential flocculation or clay mineral stability. Instead, the reduction in kaolinite abundance, as well as chlorite abundance, is probably due to the dilution of the estuarine clay-mineral assemblage by the local erosion of Ravenglass Till.

The distribution of both clay minerals and depositional environments is strongly controlled by estuarine hydrodynamics. However, a key finding of this study is that clay mineral distribution patterns are heterogeneous even within a single depositional environment, for example foreshore deposits (Figs 13 to 17); consequently, there is little statistical difference in the relative abundance of specific clay minerals, between different depositional environments (Table 7). As a result, clay mineral distribution patterns are only partly explained by an understanding of depositional environment. Instead, knowledge of local specific conditions, such as the distribution of local sediment sources and the relative importance of marine (waves and tides) and fluvial processes is required.

Early diagenetic control on clay mineral distribution

Sedimentary systems are geochemically active with the possibility of weathering processes that commenced in soils, such as feldspar alteration, and Fe–Mg-mineral alteration, continuing into the realm of sediment accumulation. It is also possible that sites of sediment transport and deposition involve totally new geochemical conditions that lead to a new suite of mineral reactions. Marginal marine settings are especially significant since they involve terrigenous sediment and low salinity, relatively organic-rich and iron-rich continental waters meeting marine conditions with their high salinity, high aqueous

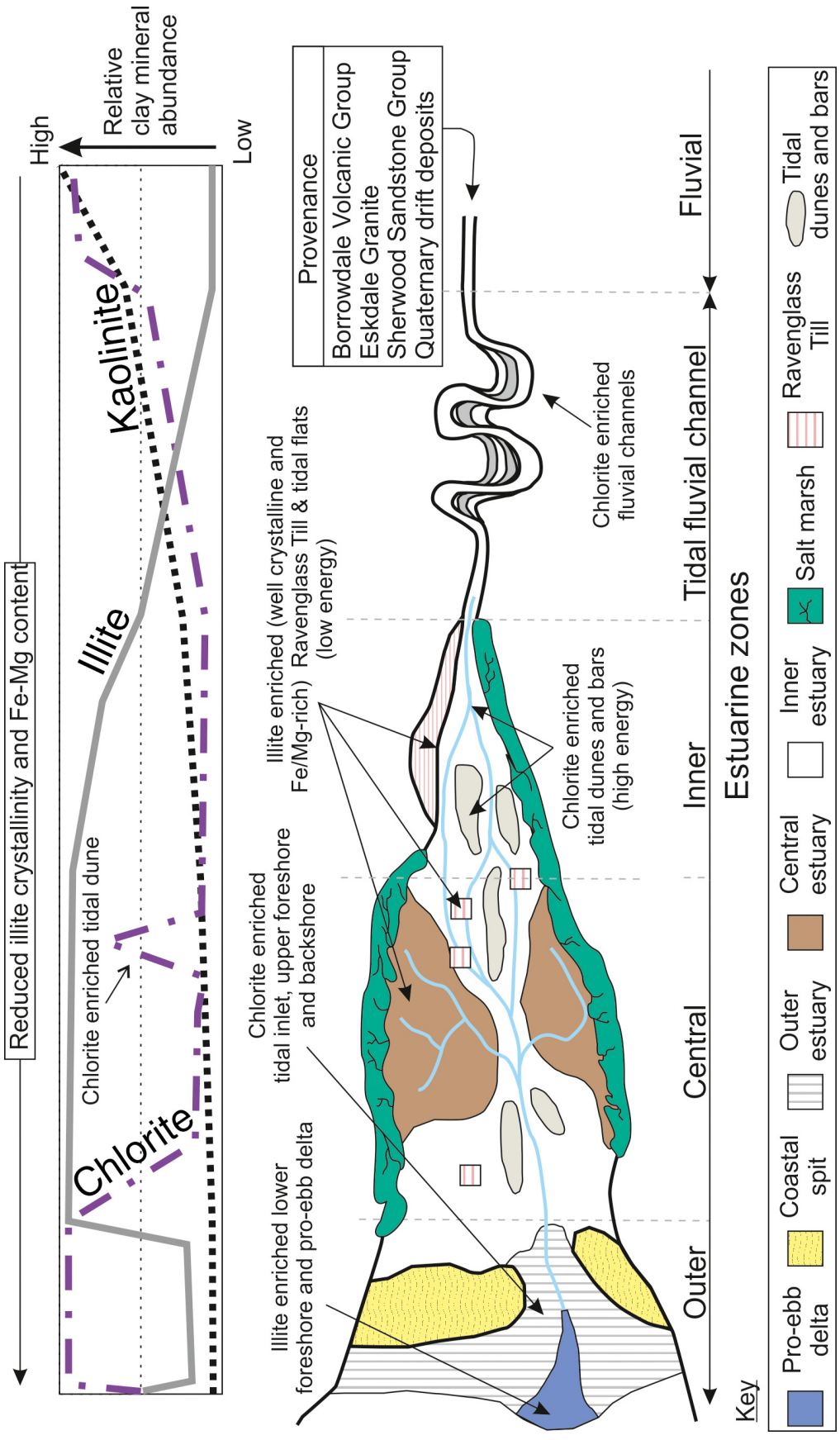

Fig. 19. Generalised model depicting the major clay mineral distribution patterns observed in the Ravenglass Estuary. Chlorite is most abundant in fluvial and outer estuarine sediments. Inner estuarine tidal bars and dunes are also relatively enriched in chlorite. Kaolinite abundance is highest in fluvial sediments and relatively homogenous in tidally-influenced estuarine sediment. Illite is most abundant in the central basin. Illite crystallinity and Fe–Mg content reduces towards the open sea. Enrichment of chlorite in fluvial sediments reflects the drainage of chloritic bedrock. Enrichment of Fe–Mg-rich illite in the central basin reflects the local erosion of Ravenglass Till.

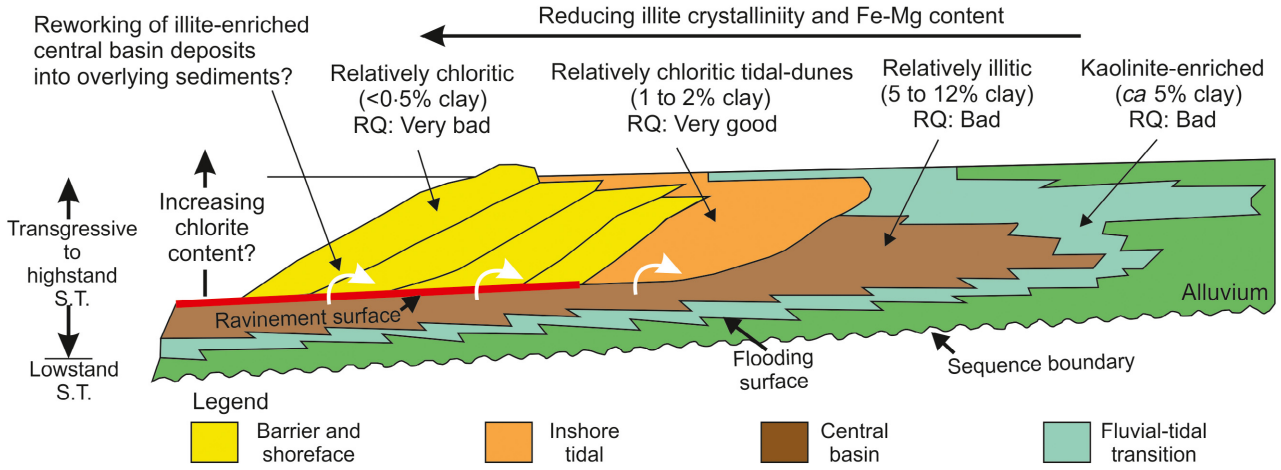

Fig. 20. Generalised sequence stratigraphic populated with relative clay mineral abundance and total clay, as well as the predicted reservoir quality (RQ) assuming a at least 1 to 2% clay is needed to form complete grain coats, after Bloch *et al.* (2002). White arrows indicate the reworking of underlying illite-rich central basin deposits into overlying chlorite-rich barrier, shoreface and inshore tidal deposits. An increase in chlorite in younger deposits is postulated following the progressive removal of illite-rich glacial deposits in the hinterland and subsequent increase in the supply of chlorite-rich fluvial sediment. The estuarine sequence stratigraphy schematic sections has been adapted from Dalrymple *et al.* (1992).

sulphate concentration and locally low oxidation state, and low pCO_2 waters (Boyle *et al.*, 1974, 1977; Sholkovitz, 1978; Berner & Berner, 2012). Significant diagenetic reactions involving clay synthesis, Fe-reduction and even silica precipitation have been described in marginal marine sediments (Michalopoulos & Aller, 1995, 2004; Aller & Michalopoulos, 1999; Michalopoulos *et al.*, 2000). Some have described physico-chemical processes of mineral alteration in marginal marine settings (Grim & Johns, 1954; Griffin & Ingram, 1955; Powers, 1957; Nelson, 1960; Daneshvar & Worden, 2018). Others have invoked a significant role for macrobenthos in sediment mineral reactions, such as during sediment bioturbation (ingestion and excretion) by the common lugworm (*Arenicola marina*); animal–sediment interaction has been reported to lead to the formation of new clay minerals (McIlroy *et al.*, 2003; Needham *et al.*, 2004, 2005; Worden *et al.*, 2006). In contrast, other studies have suggested that clay minerals undergo negligible transformation in sedimentary environments (Carroll & Starkey, 1958; Chamley, 1989; Rateev *et al.*, 2008).

Based on high-resolution QEMSCAN (SEM–EDS imaging), evidence of a small number of samples from a 1 m core from the Ravenglass Estuary, Daneshvar & Worden (2018) suggested that detrital K-feldspar grains are preferentially rimmed by neoformed illite, while plagioclase grains may be preferentially rimmed by neoformed kaolinite. It is possible that these host-specific clay mineral rims are the result of continued alteration of the recent sediment with K-feldspar altering to K-rich illite with K-free plagioclase altering to K-free kaolinite. However, it has also been reported that illite and kaolinite have formed due to intense alteration of feldspars in the hinterland (Moseley, 1978; Young *et al.*, 1986; Quirke *et al.*, 2015) (Table 1). It is conceivable that the relationship between feldspars and clay-minerals in the estuary may, alternatively, be due to the transportation and deposition of kaolinised plagioclase, and illitised K-feldspars from the hinterland and are thus an inherited feature of the sediment.

This study has mapped out the distribution of lugworms by counting faecal casts per m^2 (Fig. 8D) to test whether lugworm bioturbation may explain clay mineral abundance, as documented in laboratory studies (McIlroy *et al.*, 2003; Needham *et al.*, 2004; Worden *et al.*, 2006). However, there appears to be no spatial relationship between the distribution of the clay minerals and the distribution of lugworms in the Ravenglass Estuary (compare Fig. 8D to Fig. 12). Statistical analysis of the covariance between lugworm distribution and clay minerals confirms that there is no correlation in the Ravenglass Estuary (Table 6). The case for an early diagenetic control on clay mineral distribution patterns (Fig. 12)

remains unproven with local provenance and hydrodynamic controls potentially sufficient to explain clay distribution patterns.

Significance: reservoir quality prediction

Local-specific conditions (for example, wave-direction and tidal-range) exert a strong control on clay-mineral distribution patterns in the Ravenglass Estuary. For example, chlorite has been locally concentrated by wave energy, dominated by the prevailing south-westerly wind, onto the northern part of the foreshore (Fig. 13). As a result, in order to accurately predict clay mineral distribution in the subsurface, local-specific conditions (for example, wave-direction) need to be accounted for when quantifying risk, although it is acknowledged that these may be potentially difficult to define based on core data. However, in order to construct useful generalised models, which may be applied to a wide range of estuarine sandstones, it is first necessary to distil away all local variability unique to the Ravenglass Estuary.

Two generalised models have been developed here in order to help predict the spatial (Fig. 19; plan view) and temporal (Fig. 20; sequence stratigraphic framework) distribution of clay minerals in estuarine sandstones. Furthermore, since the ability of a clay coat to inhibit quartz cementation depends not only on mineralogy but also on the fraction of the sand grain-surface covered by clay minerals (grain coat coverage), the total abundance of clay is also critical (Billault *et al.*, 2003; Lander *et al.*, 2008; Ajdukiewicz & Larese, 2012). Bloch *et al.* (2002) reported that as little as 1 to 2% of the rock volume as clay can form extensive coats on individual sand grains. However, Pittman *et al.* (1992) suggested an optimum range of 5 to 12% sediment volume as clays for the Tuscaloosa Formation and 4 to 7% for the Berea Sandstone. As a result, generalised models presented in this study (Figs 19 and 20), which predict estuarine sandstone reservoir quality, are based on the suggested volumes of clay necessary to form grain coats (stated above), as well as clay mineral distribution patterns (this study) and detrital clay coat distribution patterns reported in the Ravenglass Estuary (Wooldridge *et al.*, 2017a,b). It should be noted that the generalised models assume that detrital chlorite, illite and kaolinite are direct precursors to burial-diagenetic chlorite, illite and kaolinite, respectively. Outer estuarine sediments are relatively chlorite-enriched, however due to a paucity of clay grade material (<0·5%) to form complete grain coats, such sandstones are likely to be heavily quartz cemented in deeply-buried (burial-temperatures exceeding 80 to 100°C) sandstone reservoirs (Figs 19 and 20). In contrast, it is suggested here that inner-estuarine, chlorite-rich tidal bars and dunes (*ca* 1% total clay; Figs 19 and 20) are likely to have the best sandstone reservoir quality with the greatest inhibition of quartz cement. Furthermore, inner estuarine tidal flats are likely to be relatively illitic (Figs 19 and 20) which is likely to block pore-throats and may exacerbate quartz grain pressure solution and subsequent quartz cementation (Oelkers *et al.*, 1996).

On a sequence-stratigraphic scale (Fig. 20), estuaries that have been previously subjected to glaciation may become progressively chlorite-enriched (better reservoir quality in younger deposits) after illite-rich drift deposits have been actively eroded away or blanketed by newly eroded material from the chlorite-rich hinterland. Furthermore, reworking of illite-rich central basin deposits into overlying inshore tidal, barrier and shoreface deposits is likely to lead to an increase in illite-rich sediment towards the base of the succession (Fig. 20). In the Ravenglass Estuary, once the influence of the Holocene drift deposits has been lost, the estuary sediment will presumably revert to a more chlorite-rich composition as currently found in the estuary hinterlands (Table 4). The relative values of the chlorite index (Figs 13 and 20) are likely to at least double, or maybe even treble (for example, approaching 0·6 as shown in Table 4), when the sediment supply is, once again, fluvial-dominated as opposed to glacial till-dominated.

CONCLUSIONS

1 Sediment supply and residence time have played major roles in controlling clay mineralogy in the Ravenglass Estuary. Chlorite-dominated sediment is derived from the hinterland via the rivers, whilst illite-dominated estuarine sediments reflect the erosion of glacial till within and around the estuary. Furthermore, despite the difference in sediment supply (southern Esk arm predominantly draining granite; northern Irt arm primarily draining andesite and red bed sandstones) from the main rivers

feeding the estuary, due to intense estuarine mixing and dilution from glacial till sediment, counterpart inner estuarine zones (inner Irt and Esk) show no significant difference in clay mineral proportions. The presence of deposits such as glacial till (or other sediments that can have long residence times in the hinterland) might have been overlooked in provenance studies of ancient systems, but are shown here to exert a major control on the clay mineral assemblage and mineral distribution patterns of a modern estuary.

2 Illite is the most abundant clay mineral in all parts of the Ravenglass Estuary, and is concentrated and most Fe–Mg-rich in fine-grained depositional environments in the inner estuary and central basin, i.e. mud flats and mixed flats. Connectivity between the illite-rich inner estuary and central basin and the southern foreshore via the ebb channel, has led to an increased concentration of illite upon the southern foreshore.

3 Chlorite and Al-rich illite typically increase in abundance with an increase in grain size corresponding to high energy depositional environments, i.e. tidal bars and dunes and outer estuarine sediment. Wave-direction originating from the south-west further concentrated chlorite upon the northern foreshore.

4 Kaolinite is relatively homogenous throughout the estuary with a slight increase at the fluvial–marine interface and slightly depleted in outer estuarine sediment. There is no relationship between bioturbation intensity (density of lugworms) and the relative abundance of a chlorite, illite or kaolinite.

5 Local-specific conditions (for example, wave-direction) exert a strong control on clay-mineral distribution patterns in the Ravenglass Estuary; however, there are general conclusions which may be applied to all estuarine sandstones. In ancient and deeply-buried sandstones, subject to burial temperatures exceeding 80 to 100°C, reservoir quality is probably best in chlorite-enriched tidal dunes and bars in the inner estuary. Despite being relatively chlorite enriched, outer estuarine sediments are likely to be heavily quartz cemented due to a paucity of the absolute quantity of clay grade material (<0·5%) that could form complete grain coats. An abundance of illite in finer-grained mud-flats and mixed-flats in the inner estuary and central basin is likely to lead to relatively low porosity and permeability and may exacerbate pressure-dissolution and subsequent quartz cementation.

ACKNOWLEDGEMENTS

This work was undertaken as part of the Chlorite Consortium at the University of Liverpool, sponsored by BP, Shell, Equinor, Eni, Chevron, Woodside and Petrobras. We thank Jenny Omma, Stuart Jones and Christopher Stevenson for their detailed and constructive comments which have helped improve this manuscript. We would also like to thank Robert Wilcox, Max Taylor, Amelia Tustin and Joanne Jeffreys for their assistance in collecting grain-size and bioturbation data.

REFERENCES

Aagaard, P., **Jahren, J.S.**, **Harstad, A.O.**, **Nilsen, O.** and **Ramm, M.** (2000) Formation of grain-coating chlorite in sandstones. Laboratory synthesized vs. natural occurrences. *Clay Mineral.*, **35**, 261–269.

Ajdukiewicz, J.M. and **Larese, R.E.** (2012) How clay grain coats inhibit quartz cement and preserve porosity in deeply buried sandstones: observations and experiments. *Am. Assoc. Petrol. Geol. Bull.*, **96**, 2091–2119.

Aller, R.C. and **Michalopoulos, P.** (1999) *Invited lecture: Tropical, mobile mud belts as global diagenetic reactors*, pp. 289–292.

Assinder, D.J., **Kelly, M.** and **Aston, S.R.** (1985) Tidal variations in dissolved and particulate phase radionuclide activities in the Esk Estuary, England, and their distribution coefficients and particulate activity fractions. *J. Environ. Radioactiv.*, **2**, 1–22.

Berner, E.K. and **Berner, R.A.** (2012) *Global Environment: Water, Air and Geochemical Cycles*, 2nd edn. Princeton University Press, Princeton, NJ, 444 pp.

Biddle, P. and **Miles, J.** (1972) The nature of contemporary silts in British estuaries. *Sed. Geol.*, **7**, 23–33.

Billault, V., **Beaufort, D.**, **Baronnet, A.** and **Lacharpagne, J.C.** (2003) A nanopetrographic and textural study of grain-coating chlorites in sandstone reservoirs. *Clay Mineral.*, **38**, 315–328.

Bloch, S., **Lander, R.H.** and **Bonnell, L.** (2002) Anomalously high porosity and permeability in deeply buried sandstone reservoirs: origin and predictability. *Am. Assoc. Petrol. Geol. Bull.*, **86**, 301–328.

Blott, S.J. and **Pye, K.** (2001) GRADISTAT: a grain size distribution and statistics package for the analysis of unconsolidated sediments. *Earth Surf. Proc. Land.*, **26**, 1237–1248.

Borchers, A., **Voigt, I.**, **Kuhn, G.** and **Diekmann, B.** (2011) Mineralogy of glaciomarine sediments from the Prydz Bay–Kerguelen region: relation to modern depositional environments. *Antarct. Sci.*, **23**, 164–179.

Bousher, A. (1999). Basic characteristics and evaluation of restoration options.

Bout-Roumazeilles, V., **Riboulleau, A.**, **Châtelet, E.A.**, **Lorenzoni, L.**, **Tribovillard, N.**, **Murray, R.W.**, **Müller-Karger, F.** and **Astor, Y.M.** (2013) Clay mineralogy of surface sediments as a tool for deciphering river contributions to the Cariaco Basin (Venezuela). *J. Geophys. Res. Oceans*, **118**, 750–761.

Boyle, E., **Collier, R.**, **Dengler, A.T.**, **Edmond, J.M.**, **Ng, A.C.** and **Stallard, R.F.** (1974) Chemical mass balance in estuaries. *Geochim. Cosmochim. Acta*, **38**, 1719–1728.

Boyle, E.A., **Edmond, J.M.** and **Sholkovitz, E.R.** (1977) Mechanism of iron removal in estuaries. *Geochim. Cosmochim. Acta*, **41**, 1313–1324.

Brockamp, O. and **Zuther, M.** (2004) Changes in clay mineral content of tidal flat sediments resulting from dike construction along the Lower Saxony coast of the North Sea, Germany. *Sedimentology*, **51**, 591–600.

Carr, A.P. and **Blackley, M.W.L.** (1986) Implications of sedimentological and hydrological processes on the distribution of radionuclides: the example of a salt marsh near Ravenglass, Cumbria. *Estuar. Coast. Shelf Sci.*, **22**, 529–543.

Carroll, D. and **Starkey, H.C.** (1958) Effect of sea-water on clay minerals. In: Clays and Clay Minerals., 7th Natational conference. Pergamon, Oxford, pp. 80–101. Elsevier.

Chamley, H. (1989) *Clay Sedimentology*. Springer-Verlag, Berlin, Germany, 560 pp.

Chung, F.H. (1974a) Quantitative interpretation of X-ray diffraction patterns of mixtures: 1. Matrix-flushing method for quantitative multicomponent analysis. *J. Appl. Crystallogr.*, **7**, 519–525.

Chung, F.H. (1974b) Quantitative interpretation of X-ray diffraction patterns of mixtures: 2. Adiabatic principle of X-ray diffraction analysis of mixtures. *J. Appl. Crystallogr.*, **7**, 526–531.

Dalrymple, R.W., **Zaitlin, B.A.** and **Boyd, R.** (1992) Estuarine facies models - conceptual models and stratigraphic implications. *J. Sed. Petrol.*, **62**, 1130–1146.

Daneshvar, E. (2015) Dissolved iron behavior in the Ravenglass Estuary waters, an implication on the early diagenesis. *Univ. J. Geosci.*, **3**, 1–12.

Daneshvar, E. and **Worden, R.H.** (2018) Feldspar alteration and Fe minerals: origin, distribution and implications for sandstone reservoir quality in estuarine sediments. In: *Reservoir Quality Prediction in Sandstones and Carbonates* (Eds P.J. Armitage, A. Butcher, J. Churchill, A. Csoma, C. Hollis, R.H. Lander, J. Omma and R.H. Worden). *Geol. Soc. London Spec. Publ.*, **435**, 123–139.

Dowey, P.J., **Hodgson, D.M.** and **Worden, R.H.** (2012) Pre-requisites, processes, and prediction of chlorite grain coatings in petroleum reservoirs: a review of subsurface examples. *Mar. Pet. Geol.*, **32**, 63–75.

Dowey, P.J., **Worden, R.H.**, **Utley, J.** and **Hodgson, D.M.** (2017) Sedimentary controls on modern sand grain coat formation. *Sed. Geol.*, **353**, 46–63.

Du Chatelet, E.A., **Bout-Roumazeilles, V.**, **Coccioni, R.**, **Frontalini, F.**, **Francescangeli, F.**, **Margaritelli, G.**, **Rettori, R.**, **Spagnoli, F.**, **Semprucci, F.** and **Trentesaux, A.** (2016) Environmental control on a land–sea transitional setting: integrated sedimentological, geochemical and faunal approaches. *Environ. Earth Sci.*, **75**, 123.

Eberl, D.D., **Farmer, V.C.** and **Barrer, R.M.** (1984) Clay mineral formation and transformation in rocks and soils [and Discussion]. *Phil. Trans. Roy. Soc. London A Math. Phys. Eng. Sc.*, **311**, 241–257.

Edzwald, J.K. and **O'Mella, C.R.** (1975) Clay distributions in recent estuarine sediments. *Clays Clay Mineral.*, **23**, 39–44.

Ehrenberg, S.N. (1993) Preservation of anomalously high-porosity in deeply buried sandstones by grain coating chlorite - examples from the Norwegian continental shelf. *Am. Assoc. Petrol. Geol. Bull.*, **77**, 1260–1286.

Esquevin, J. (1969) Influence de la composition chimique des illites sur leur cristallinité. *Bull. Centre Recherche Elf Pau-SNPA*, **3**, 147–153.

Feuillet, J.-P. and **Fleischer, P.** (1980) Estuarine circulation; controlling factor of clay mineral distribution in James River Estuary, Virginia. *J. Sed. Petrol.*, **50**, 267–279.

Folk, R.L. and **Ward, W.C.** (1957) Brazos river bar. A study in the significance of grain size parameters. *J. Sed. Petrol.*, **27**, 3–26.

Gibbs, R.J. (1977) Clay mineral segregation in the marine environment. *J. Sed. Res.*, **47**, 237–243.

Gingele, F.X., **De Deckker, P.** and **Hillenbrand, C.-D.** (2001) Clay mineral distribution in surface sediments between Indonesia and NW Australia—source and transport by ocean currents. *Mar. Geol.*, **179**, 135–146.

Griffin, G.M. and **Ingram, R.L.** (1955) Clay minerals of the Neuse River estuary. *J. Sed. Res.*, **25**, 194–200.

Griffiths, J., **Worden, R.H.**, **Wooldridge, L.J.**, **Utley, J.E.** and **Duller, R.A.** (2018a) Compositional variation in modern estuarine sands: predicting major controls on sandstone reservoir quality. *AAPG Bull.*

Griffiths, J., **Worden, R.H.**, **Wooldridge, L.J.**, **Utley, J.E.** and **Duller, R.A.** (2018b) Detrital clay coats, clay minerals, and pyrite: a modern shallow-core analogue for ancient and deeply buried estuarine sandstones. *J. Sed. Res.*, **88**, 1205–1237.

Grim, R.E. and **Johns, W.D.** (1954) Clay mineral investigations of sediments in the northern Gulf of Mexico. *Clays Clay Mineral.*, **2**, 81–103.

Grim, R.E., **Bray, R.H.** and **Bradley, W.F.** (1937) The mica in argillaceous sediments. *Am. Mineral.*, **22**, 813–829.

Hathaway, J.C. (1972) Regional clay mineral fades in estuaries and continental margin of the United States east coast. In: *Environmental Framework of Coastal Plain Estuaries* (Ed. P.W. Nelson). *Geol. Soc. Am. Mem.*, **133**, 293–316.

Hillier, S. (1994) Pore-lining chlorites in siliciclastic reservoir sandstones: electron microprobe, SEM and XRD data, and implications for their origin. *Clay Mineral.*, **29**, 665–680.

Jones, S.J. (2017) Goo, glue, and grain binding: importance of biofilms for diagenesis in sandstones. *Geology*, **45**, 959–960.

Kelly, M., **Emptage, M.**, **Mudge, S.**, **Bradshaw, K.** and **Hamilton-Taylor, J.** (1991) The relationship between sediment and plutonium budgets in a small macrotidal estuary - Esk Estuary, Cumbria, UK. *J. Environ. Radioactiv.*, **13**, 55–74.

Ketzer, J.M., **Holz, M.**, **Morad, S.** and **Al-Aasm, I.** (2003) Sequence stratigraphic distribution of diagenetic alterations in coal-bearing, paralic sandstones: evidence from the Rio Bonito Formation (early Permian), southern Brazil. *Sedimentology*, **50**, 855–877.

Krumm, S. and **Buggisch, W.** (1991) Sample preparation effects on illite crystallinity measurement: grain-size gradation and particle orientation. *J. Metamorph. Geol.*, **9**, 671–677.

Kübler, B. (1964) Les argiles, indicateurs de métamorphisme. *Rev. Inst. Fr. Pétrol.*, **19**, 1093–1112.

Lander, R.H., **Larese, R.E.** and **Bonnell, L.M.** (2008) Toward more accurate quartz cement models: the importance of euhedral versus noneuhedral growth rates. *Am. Assoc. Petrol. Geol. Bull.*, **92**, 1537–1563.

Lloyd, J.M., **Zong, Y.**, **Fish, P.** and **Innes, J.B.** (2013) Holocene and Late-glacial relative sea-level change in

north-west England: implications for glacial isostatic adjustment models. *J. Quatern. Sci.*, **28**, 59–70.

McDougall, D.A. (2001) The geomorphological impact of Loch Lomond (Younger Dryas) Stadial plateau icefields in the central Lake District, northwest England. *J. Quatern. Sci.*, **16**, 531–543.

McIlroy, D., **Worden, R.H.** and **Needham, S.J.** (2003) Faeces, clay minerals and reservoir potential. *J. Geol. Soc.*, **160**, 489–493.

Meade, R.H. (1969) Landward transport of bottom sediments in estuaries of the Atlantic coastal plain. *J. Sed. Res.*, **39**, 222–234.

Merritt, J.W. and **Auton, C.A.** (2000) An outline of the lithostratigraphy and depositional history of Quaternary deposits in the Sellafield district, west Cumbria. *Proc. Yorks. Geol. Soc.*, **53**, 129–154.

Michalopoulos, P. and **Aller, R.C.** (1995) Rapid clay mineral transformation in Amazon Delta sediments - reverse weathering and oceanic element cycles. *Science*, **270**, 614–617.

Michalopoulos, P. and **Aller, R.C.** (2004) Early diagenesis of biogenic silica in the Amazon delta: alteration, authigenic clay formation, and storage. *Geochim. Cosmochim. Acta*, **68**, 1061–1085.

Michalopoulos, P., **Aller, R.C.** and **Reeder, R.J.** (2000) Conversion of diatoms to clays during early diagenesis in tropical, continental shelf muds. *Geology*, **28**, 1095–1098.

Moore, D.M. and **Reynolds, R.C.** (1997) *X-ray Diffraction and the Identification and Analysis of Clay Minerals*. Oxford University Press, Oxford, UK, 378 pp.

Morad, S., **Ketzer, M.** and **de Ros, L.F.** (2013) Linking diagenesis to sequence stratigraphy: An integrated tool for understanding and predicting reservoir quality distribution. In: *Linking Diagenesis to Sequence Stratigraphy* (Eds S. Morad, J.M. Ketzer and L.F. De Ros) John Wiley & Sons, West Sussex, UK.

Moseley, F. (1978) *The Geology of the Lake District*. Yorkshire Geological Society, 284 pp.

Needham, S.J., **Worden, R.H.** and **McIlroy, D.** (2004) Animal-sediment interactions: the effect of ingestion and excretion by worms on mineralogy. *Biogeosciences*, **1**, 113–121.

Needham, S.J., **Worden, R.H.** and **McIlroy, D.** (2005) Experimental production of clay rims by macrobiotic sediment ingestion and excretion processes. *J. Sed. Res.*, **75**, 1028–1037.

Neiheisel, J. and **Weaver, C.E.** (1967) Transport and deposition of clay minerals southeastern United States. *J. Sed. Res.*, **37**, 1084–1116.

Nelson, B.W. (1960) Clay mineralogy of the bottom sediments, Rappahannock River, Virginia. In: Clays and Clay Minerals: Proceedings of the Seventh National Conference on Clays and Clay Minerals, pp. 135–148.

Oelkers, E.H., **Bjorkum, P.A.** and **Murphy, W.M.** (1996) A petrographic and computational investigation of quartz cementation and porosity reduction in North Sea sandstones. *Am. J. Sci.*, **296**, 420–452.

Oliveira, A., **Rocha, F.**, **Rodrigues, A.**, **Jouanneau, J.**, **Dias, A.**, **Weber, O.** and **Gomes, C.** (2002) Clay minerals from the sedimentary cover from the Northwest Iberian shelf. *Prog. Oceanogr.*, **52**, 233–247.

Pittman, E.D., **Larese, R.E.** and **Heald, M.T.** (1992) Clay coats: occurrence and relevance to preservation of porosity in sandstones. In: *Origin, Diagenesis and Petrophysics of Clay Minerals in Sandstones* (Eds D.W. Houseknecht and E.D. Pittman), *SEPM Spec. Publ.*, **47**, 241–255.

Posamentier, H.W. and **Walker, R.G.** (eds.) (2006) *Facies Models Revisited*. SEPM Special Publication, Oklahoma.

Postma, H. (1967) Sediment transport and sedimentation in the estuarine environment. In: *Estuaries* (Ed. G.H. Lauff), pp. 158–184. American Association for the Advancement of Science, Washington, DC.

Powers, M.C. (1957) Adjustment of land derived clays to the marine environment. *J. Sed. Res.*, **27**, 355–372.

Pye, K. and **Blott, S.J.** (2014) The geomorphology of UK estuaries: the role of geological controls, antecedent conditions and human activities. *Estuar. Coast. Shelf Sci.*, **150**, 196–214.

Quirke, J., **Henderson, C.M.B.**, **Pattrick, R.A.D.**, **Rosso, K.M.**, **Dent, A.**, **Sharples, J.W.** and **Pearce, C.I.** (2015) Characterizing mineralogy and redox reactivity in potential host rocks for a UK geological disposal facility. *Mineral. Mag.*, **79**, 1353–1367.

R Core Team (2016) *R: A Language and Environment for Statistical Computing*. R Foundation for Statistical Computing, Vienna, Austria.

Rateev, M.A., **Sadchikova, T.A.** and **Shabrova, V.P.** (2008) Clay minerals in recent sediments of the World Ocean and their relation to types of lithogenesis. *Lithol. Min. Resour.*, **43**, 125–135.

Rudert, M. and **Müller, G.** (1981) Mineralogy and provenance of suspended solids in estuarine and near-shore areas of the southern North Sea. *Senckenb. Marit*, **13**, 57–64.

Salem, A.M., **Morad, S.**, **Mato, L.F.** and **Al-Aasm, I.S.** (2000) Diagenesis and reservoir-quality evolution of fluvial sandstones during progressive burial and uplift: evidence from the Upper Jurassic Boipeba Member, Reconcavo basin, northeastern Brazil. *Am. Assoc. Petrol. Geol. Bull.*, **84**, 1015–1040.

Sholkovitz, E.R. (1978) The floculation of dissolved Fe, Mn, Al, Cu, Ni, Co and Cd during estuarine mixing. *Earth Planet. Sci. Lett.*, **41**, 77–86.

Simpson, B. (1934) The petrology of the Eskdale (Cumberland) granite. *Proc. Geol. Assoc.*, **45**, 17–34.

Skarpeid, S.S., **Churchill, J.M.**, **Hilton, J.P.J.**, **Izatt, C.N.** and **Poole, M.T.** (2017) The Knarr Field: a new development at the northern edge of the North Sea. In: Geological Society, London, Petroleum Geology Conference series, 8, pp. PGC8. 23. Geological Society of London.

Stone, P. and **Merriman, R.J.** (2004) Basin thermal history favours an accretionary origin for the Southern Uplands terrane, Scottish Caledonides. *J. Geol. Soc.*, **161**, 829–836.

Stricker, S. and **Jones, S.J.** (2016) Enhanced porosity preservation by pore fluid overpressure and chlorite grain coatings in the Triassic Skagerrak, Central Graben, North Sea, UK. *Geol. Soc. Lond. Spec. Publ.*, **435**, SP435.4.

Strong, G.E., **Milodowski, A.E.**, **Pearce, J.M.**, **Kemp, S.J.**, **Prior, S.V.** and **Morton, A.C.** (1994) The petrology and diagenesis of Permo-Triassic rocks of the Sellafield area, Cumbria. In: Proceedings of the Yorkshire Geological and Polytechnic Society, 50, pp. 77–89. Geological Society of London.

Virolle, M., **Brigaud, B.**, **Bourillot, R.**, **Féniès, H.**, **Portier, E.**, **Duteil, T.**, **Nouet, J.**, **Patrier, P.** and **Beaufort, D.** (2018) Detrital clay grain coats in estuarine clastic deposits: origin and spatial distribution within a modern sedimentary system, the Gironde Estuary (south-west France). *Sedimentology*.

Watson, D.F. and **Philip, G.M.** (1985) Comment on "a nonlinear empirical prescription for simultaneously

interpolating and smoothing contours over an irregular grid" by F. Duggan. *Comput. Meth. Appl. Mech. eEng.*, **50**, 195–198.

Whitehouse, U.G., **Jeffrey, L.M.** and **Debbrecht, J.D.** (1960) Differential settling tendencies of clay minerals in saline waters. *Clays Clay Mineral.*, **7**, 1–79.

Windom, H.L. (1976) Lithogenous material in marine sediments. *Chem. Oceanogr.*, **5**, 103–135.

Wooldridge, L.J., **Worden, R.H.**, **Griffiths, J.**, **Thompson, A.** and **Chung, P.** (2017a) Biofilm origin of clay-coated sand grains. *Geology*, **45**, 875–878.

Wooldridge, L.J., **Worden, R.H.**, **Griffiths, J.** and **Utley, J.E.P.** (2017b) Clay-coated sand grains in petroleum reservoirs: understanding their distribution via a modern analogue. *J. Sed. Res.*, **87**, 338–352.

Worden, R.H. and **Morad, S.** (2003) Clay minerals in sandstones: controls on formation, distribution and evolution. In: *Clay Mineral Cements in Sandstones* (Eds R.H. Worden and S. Morad), *Int. Assoc. Sed. Spec. Publ.*, **34**, 3–41.

Worden, R.H., **Needham, S.J.** and **Cuadros, J.** (2006) The worm gut; a natural clay mineral factory and a possible cause of diagenetic grain coats in sandstones. *J. Geochem. Explor.*, **89**, 428–431.

Worden, R., **Armitage, P.**, **Butcher, A.**, **Churchill, J.**, **Csoma, A.**, **Hollis, C.**, **Lander, R.** and **Omma, J.** (2018) Petroleum reservoir quality prediction: overview and contrasting approaches from sandstone and carbonate communities. In: *Reservoir Quality Prediction in Sandstones and Carbonates* (Eds P.J. Armitage, A. Butcher, J. Churchill, A. Csoma, C. Hollis, R.H. Lander, J. Omma and R.H. Worden), *Geol. Soc. London Spec. Publ.*, **435**, 1–31.

Young, B., **Fortey, N.J.** and **Nancarrow, P.H.A.** (1986) An occurrence of tungsten mineralisation in the Eskdale Intrusion, West Cumbria. *Proc. Yorks. Geol. Soc.*, **46**, 15–21.

Manuscript received 13 September 2017; revision accepted 7 December 2018